Australia's National
Science Agency

Defining the Geometry of the Saltwater Interface at Coffin Bay, SA using Airborne EM

TJ Munday, C Sorensen and T Ibrahimi

1 November 2025

Report prepared for Department of Environment and Water, South Australia.

CSIRO Report #: EP2025-0066

Government of South Australia
Department for Environment and Water

CSIRO Mineral Resources

Citation

Munday TJ, Sorensen, C and Ibrahimi, T (2024) Defining the Geometry of the Saltwater Interface at Coffin Bay, SA using Airborne EM. CSIRO report #: EP2025-0066, CSIRO, Australia. 52pp.

Copyright

© Commonwealth Scientific and Industrial Research Organisation 2024. To the extent permitted by law, all rights are reserved and no part of this publication covered by copyright may be reproduced or copied in any form or by any means except with the written permission of CSIRO.

Important disclaimer

CSIRO advises that the information contained in this publication comprises general statements based on scientific research. The reader is advised and needs to be aware that such information may be incomplete or unable to be used in any specific situation. No reliance or actions must therefore be made on that information without seeking prior expert professional, scientific and technical advice. To the extent permitted by law, CSIRO (including its employees and consultants) excludes all liability to any person for any consequences, including but not limited to all losses, damages, costs, expenses and any other compensation, arising directly or indirectly from using this publication (in part or in whole) and any information or material contained in it.

CSIRO is committed to providing web accessible content wherever possible. If you are having difficulties with accessing this document please contact tim.munday@csiro.au

Contents

Contents 1

1 Introduction 5

1.1 Background 5

1.2 Objectives 5

2 AEM System and Data 6

2.1 AEM systems 6

2.2 AEM Survey 8

3 AEM Data Modelling and Inversion 9

3.1 Data processing 9

3.2 Modelling and inversion 10

4 Derived Products 16

4.1 Interval conductivities 16

4.2 Conductivity-depth sections 19

4.3 Saltwater Interface 20

5 Summary 28

6 Recommendations 28

7 References 30

Figures

Figure 2-1: Principles of time domain EM data acquisition for a fixed-wing EM system such as TEMPEST 7

Figure 2-2: The TEMPEST AEM system in survey mode over the Eyre Peninsula. The transmitter loop, draped around the wingtips, tail and nose of the aircraft is defined, while the receiver coils, hosted in fibreglass bird, are towed approximately 120m behind and below the aircraft. . 7

Figure 2-3: Regional setting of study area with the extent of the historical TEMPEST AEM flight lines defined in red. The focus for this study was the area demarked by the red rectangle. 8

Figure 2-4: TEMPEST flight line map overlain on true colour satellite image of the Coffin Bay area. The area for this study is defined by the red rectangle. The flight lines re-inverted for this Project are numbered. The locations of key monitoring bores are also shown. 9

Figure 3-1: Schematic representation of TEMPEST fixed-wing time domain EM data acquisition and interpretation. A) Data are acquired along parallel flight lines, with data recorded at fixed

time intervals (soundings) along each flight line; B) The EM receiver (housed in a “bird”) towed behind and below the transmitter, measures the ground response as a function of time; C) The measured response is used to determine how conductivity structure varies with depth by transformation or inversion. Conductivity-depth values can be calculated for each observation, taking account of the elevation and geometry of the system above the ground; D) The modelled conductivity structure for each sounding can then gridded into conductivity-depth intervals to provide a spatial representation of the subsurface conductivity structure at different depths below the ground surface. These maps can be shown as elevations (mAHD) or as depth intervals below the ground surface ground surface; E) Individual soundings from a flight line or transect of several soundings may also be stitched together into conductivity-depth sections to provide a representation of the 2D variation of conductivity (a conductivity-depth section), sometimes referred to as a “para-section” (see also Figure 3-2). 11

Figure 3-2: Conductivity-depth sections for different inversion approaches – Line 10260. 12

Figure 3-3: Schematic representation of parameters considered and solved for in the inversion 13

Figure 3-4: Schematic overview of the process of allowing prior information to migrate along and between a series of soundings (fiducials) acquired by an AEM system when they are inverted using the Spatially Constrained Inversion (SCI) procedure. 14

Figure 3-5: Gridded image of the Depth of Investigation (DOI) for the inverted lines of TEMPEST data. 16

Figure 4-1: Example conductivity-depth intervals, for specified intervals (in metres) below the ground surface (BGS) overlain on true colour satellite imagery. The top row shows a sequence of depth intervals starting at 0-5m BGS, increasing in depth to 25-30m BGS. The lower row shows depth intervals at greater depths. Evidence of the saltwater interface progressing inland (represented by elevated conductivities) becomes clear in the 25 to 30m depth interval, with the irregularity of its landward shape becoming more apparent at greater depths. The influence of the unweathered Proterozoic basement (represented by elongate NNE-SSW resistive zones) on the geometry of the SWI and its extent inland is apparent in the deeper interval conductivities. Irregularities in the SWI, as it extends inland, may reflect lateral changes in the lithology of the Quaternary, underlying sediments and the Proterozoic basement. 17

Figure 4-2: Example conductivity-depth intervals for elevations in metres Australian Height Datum (mAHD), for specified intervals overlain on true colour satellite imagery. The top row shows a sequence of depth intervals starting at 0 mAHD, and incrementing in 5 metre intervals to 20 mAHD. The lower row of images extends the depth shown to -40 mAHD. The SWI, defined by elevated conductivities (yellows, reds and purples) is shown to extend inland from the coast and is limited in its eastward extent by a resistive (blue) basement high which strikes NNE – SSW on the eastern side of the inverted data set. 18

Figure 4-3: Conductivity-depth section for a 30 Layer, smooth SCI for Line 10260. The section is 7km long, oriented with the NW on the left. It shows a highly conductive, laterally extensive, and sub-horizontal zone on the left side of the section which is attributed to saltwater ingress into the Quaternary aquifer from the coast. The topography on the section is defined by the SRTM 1sec data. Disruption of the more conductive layers between 4000 and 6000m is

attributed to the presence of an unweathered basement ridge extending into the plane of section. 19

Figure 4-4: Conductivity-depth section for a 30 Layer, sharp SCI for Line 10260 19

Figure 4-5: A pseudo coloured conductivity-depth interval for 50-55m (BGS) overlain on a satellite image with monitoring bore locations (left panel), with inverted (Sharp model SCI inversion) soundings (right panels) from the TEMPEST data closest to bores LKW40 and LKW 57 (locations indicated on accompanying image). The results of the recently acquired borehole inductive conductivity logs (medium and deep induction are overlain on the TEMEPST models (left panels). 20

Figure 4-6: Interval conductivity image for depths of 90-95m below the ground surface, showing the sharp boundary between the conductive, saline groundwater to the west and a resistive (basement) unit to the east. The sharp boundary extends south from bore LKW63 to LKW60 and southwards from there. 21

Figure 4-7: Picked interface lines for different cut-off values for a single flight line (line 10220). Note that the elevation of the SWI decreases inland as is expected and truncates against an interpreted basement high. 22

Figure 4-8: Model of the elevation (mAHD) of the *top* of the saltwater interface derived from inverted TEMPEST data for the area inland of Coffin Bay township. The pseudo-coloured image of elevation is overlain on a Satellite image of the area. Monitoring bore locations are also detailed. The area delimited by the red dashed rectangle is reproduced in Figure 4-9. The elevation of the SWI decreases inland from the coast, and the southeastern extent is defined by the truncation of the SWI against a NNE-SSW oriented basement high. 22

Figure 4-9: Pseudo coloured model of the elevation of the upper surface of saltwater interface extending through the Quaternary aquifer beneath the Coffin Bay town water supply bore field. TEMPEST AEM flight lines are overlain, with line 10260 labelled. This line intersects the SE margin of the bore field. 23

Figure 4-10: Conductivity-depth section for a subset of flightline 10260 which transects the southwestern margin of the Coffin Bay town water supply bore field. The section covers the extent of the line shown in Figure 4-8. The relatively abrupt termination of the laterally continuous conductive feature to the southeast of the bore field strongly suggests that the interface terminates against a basement high in the southeast. 23

Figure 4-11: Conceptualisation of the Coffin Bay A lens fresh and saline groundwater interactions, illustrating the potential for saline up-coning. Figure sourced from Ward et al. (2009). 24

Figure 4-12: Elevation interval conductivity -10 to -15 mAHD 25

Figure 4-13: Elevation interval conductivity -15 to -20 mAHD 25

Figure 4-14: Elevation interval conductivity -20 to -25 mAHD 26

Figure 4-15: Elevation interval conductivity -25 to -30 mAHD 26

Figure 4-16: Elevation interval conductivity -30 to -35 mAHD 27

Figure 4-17: Elevation interval conductivity -35 to -40 mAHD 27

Figure 6-1: Proposed orientation and length of ground EM transects for the Coffin Bay town water supply bore field. Transects are plotted on a map of the elevation of the modelled saltwater interface. 29

Tables

Table 6-1 Proposed ground time domain EM transects 28

Acknowledgement

CSIRO would like to acknowledge the support of Kate Hyland the DEW team in helping progress this study, including Kent Inverarity for providing the recent downhole geophysical data. Both Kate and Kent provided valuable input into the report's finalisation and are thanked for that. Peter Baker is acknowledged for backing the idea of re-processing the existing AEM data over the area.

1 Introduction

1.1 Background

Groundwater in the Eyre Peninsula of South Australia is scarce with potable resources limited to the western coastal margin and the southern tip of the Peninsula because of slightly elevated rainfall and a suitable host rock which can recharge rapidly. These groundwater resources, often referred to as lenses, occur within the unconfined Quaternary limestone aquifer (the Bridgewater Formation). The Coffin Bay A lenses have assumed particular significance as sources of reticulated public water supply; however, they are affected by increased demand, climate change and the threat of salt-water intrusion (SWI). Whilst it is known that the Coffin Bay A lens extends under the Coffin Bay National Park (see Somaratne et al. 2009), land access for drilling is limited, making it particularly difficult to accurately define the geometry and extent and potential threat of the SWI to the lens systems and the available groundwater resource. Airborne geophysical data, specifically airborne electromagnetic (AEM) data provide an effective, non-intrusive means, for assessing the SWI in coastal settings and its potential to be a threat to available potable resources.

Airborne electromagnetics has been used in numerous studies of coastal areas to image the interaction between fresh aquifer systems that are affected by seawater intrusion. The strong conductivity contrast between fresh and saline water makes it a relatively easy target to define using electromagnetic methods. Examples of the applicability of the technology include the work of Kirkegaard et al. (2011), who used AEM data to estimate the salinity of the Ringkøbing lagoon on the west coast of Denmark. Along the border of Germany and Denmark, Jørgensen et al. (2012) employed a heli-borne AEM system to identify preferential flow paths for the movement of seawater in the region. Teatini et al. (2011) used AEM data to map the extent of hydrostratigraphic units and the presence of freshwater beneath the Venice Lagoon in northern Italy. In north-western Australia, Annetts et al. (2015) employed the TEMPEST AEM system to successfully map the variable geometry of the saltwater interface across the La Grange region in Western Australia. Pedersen et al. (2017) identified the presence of fresh and saline groundwater onshore and offshore using AEM data acquired near the coast of the Netherlands. Most recently, Goebel et al. (2019) acquired SkyTEM AEM data in the offshore region in the northern part of Monterey Bay, in California, USA to define the geometry of the saltwater interface.

For this Project, historical TEMPEST AEM data covering the southern part of the Eyre Peninsula, including the Coffin Bay area were identified as having potential to identify the extent and geometry of the saltwater-freshwater interface, and contribute to the future management of the Coffin Bay town water supply. These data were initially acquired as part of a larger hydrogeophysical investigation assessing the fresh groundwater resources of the region (see Fitzpatrick et al, 2009). The results from that survey formed part of further groundwater resource and vulnerability assessments undertaken by Ward et al. (2009) and Somaratne et al. (2009) among others.

1.2 Objectives

The specific objectives of this study were to:

1. Undertake focused reprocessing and constrained inversion of TEMPEST airborne electromagnetic (AEM) survey data acquired over the Coffin Bay area, Eyre Peninsula, South Australia, and
2. Interpret the resulting modelled conductivity structure to define the spatial extent, and geometry of the saltwater interface, and the potential threat of up-coning in the vicinity of the town water-supply bores for Coffin Bay.

2 AEM System and Data

2.1 AEM systems

The data used in this study were acquired using the TEMPEST fixed-wing time domain airborne electromagnetic system (Lane et al 2000). It is a system where the transmitter loop is draped around the wingtips, tail and nose of the aircraft while the receiver coils are hosted in a "bird" towed approximately 120m behind and below the aircraft (Figure 2-1). The transmitter height is nominally 120m above the ground. The TEMPEST system measures both the inline (X) and vertical (Z) components. The deconvolved ground response is converted to a 100% duty cycle square-wave B field response.

2.1.1 Principles of the time domain electromagnetic method

As with any time domain EM system, the principal of operation involves the generation of a primary magnetic field from the passage of an electrical current in a transmitter loop on the aircraft. When the current is turned off abruptly, the changing magnetic field induces a current in the ground that moves in circular horizontal paths and another magnetic field (the secondary field). Initially this is equal to the primary magnetic field but is rapidly weakened by the electrical resistivity of the ground and it dissipates or decays. The decaying secondary magnetic field is measured by the receiver coils (positioned at the rear and offset from the transmitter loop in the case of the TEMPEST EM system, see Figure 2-1). Whilst dissipating the current diffuses downwards and outwards, occupying an increasing volume of the subsurface. Shortly after turnoff, the current is concentrated in the near-surface and therefore the measured signal will reflect conductivities of near surface layers. With later times the current propagates deeper into the ground and the measured signal will contain information of the conductivity of these deeper layers.

The diffusion is initially quick, but it slows up with time. Diffusion is slower for conductive ground, and faster for resistive ground settings. Diffusion speed is proportional to $1/\sqrt{\sigma t}$, where t is the time after turnoff and σ is the ground conductivity. The recorded dataset (the decaying secondary magnetic field) is organised in time-windows, which are typically logarithmically increasing to improve the signal to noise ratio at later times, where the signal can be weak. The shape of the decaying signal provides information about the vertical conductivity structure of the subsurface.

2.1.2 Spatial resolution of ground and airborne EM systems

It is useful to briefly consider the resolution (vertical and lateral) of an EM system which can vary depending on the configuration of the system. As a rough guide the lateral resolution of airborne time-domain EM systems is of the order of 10's to 100's metres The spatial resolution or footprint of an EM system is the area or volume of the ground beneath the system which contributes most of the observed response. The spatial resolution of an AEM system depends on the geometry of the system, transmitted power and frequency range, receiver sensitivity and ground conductivity distribution (Reid et al. 2006). The footprint of a system can also be used to assess appropriate flight line spacing for surveys as well as the applicability of 1D interpretations. The resolution is better along lines where data density is large compared to across lines. For TEMPEST lateral resolution will be of the order of several hundred metres. Vertical resolution is dependent on the conductivity of the subsurface. However, AEM systems can resolve significant changes in the vertical conductivity structure, particularly the top of a conductor – such as a saltwater interface, within a few metres.

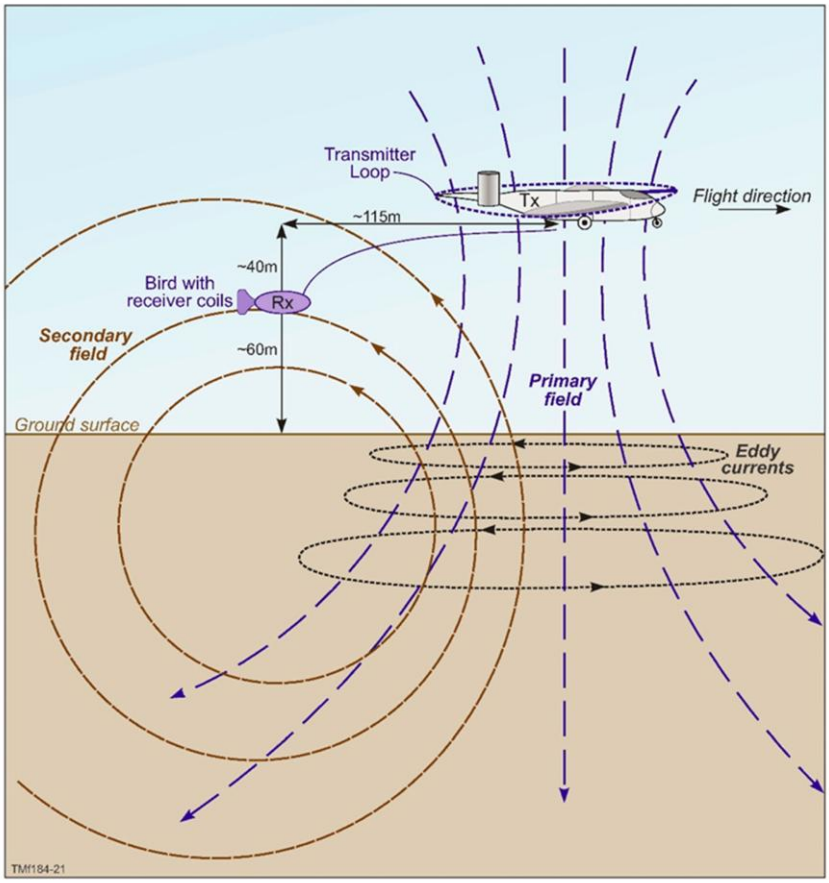


Figure 2-1: Principles of time domain EM data acquisition for a fixed-wing EM system such as TEMPEST.



Figure 2-2: The TEMPEST AEM system in survey mode over the Eyre Peninsula. The transmitter loop, draped around the wingtips, tail and nose of the aircraft is defined, while the receiver coils, hosted in fibreglass bird, are towed approximately 120m behind and below the aircraft.

2.2 AEM Survey

The TEMPEST AEM data were acquired in September 2006 by Fugro Airborne Surveys Pty Ltd on behalf of CSIRO Exploration and Mining (Lee and Stenning 2006) for SA Water. The total survey covered 1016-line kilometres, but for this current study only the northeastern part of the survey was assessed (see red rectangular area in Figure 1).

Flight lines were oriented NW-SE (140 -320 degrees) extending from Coffin Bay in the west and approximately 10km inland to the SE (Figure 2).

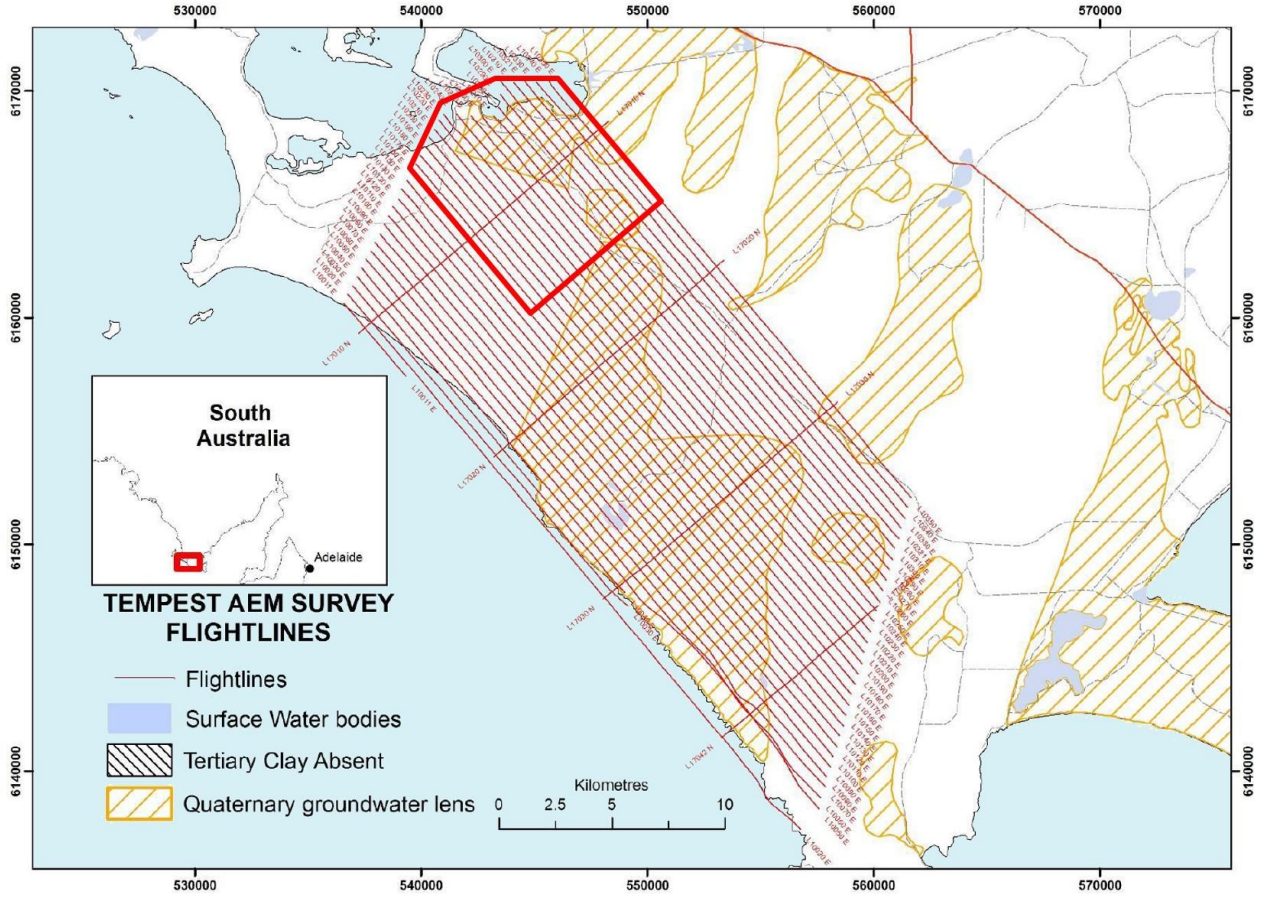


Figure 2-3: Regional setting of study area with the extent of the historical TEMPEST AEM flight lines defined in red. The focus for this study was the area demarked by the red rectangle.

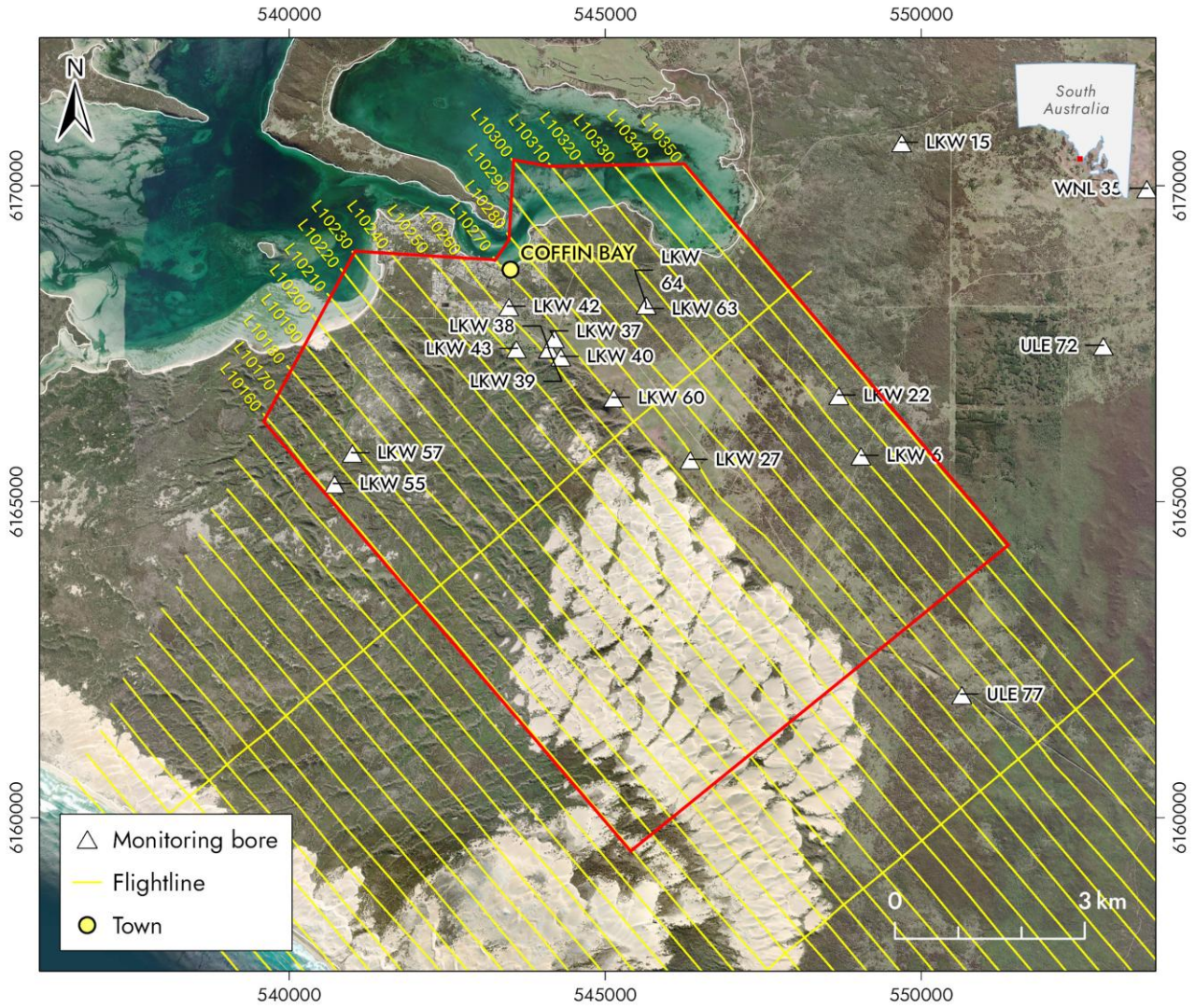


Figure 2-4: TEMPEST flight line map overlain on true colour satellite image of the Coffin Bay area. The area for this study is defined by the red rectangle. The flight lines re-inverted for this Project are numbered. The locations of key monitoring bores are also shown.

3 AEM Data Modelling and Inversion

The processing and subsequent inversion of the data was carried out using the Aarhus Workbench processing and inversion software package (Auken et al. 2015).

3.1 Data processing

The data as supplied had undergone post-processing by the contractor. The final AEM data were supplied both as geometry corrected (for a nominal system, geometry) and non-geometry corrected data. The non-geometry corrected version of the data were then imported to Aarhus Workbench. The use of uncorrected data allows the inversion methods to solve for system geometry variations (the height of the transmitter above the ground along with its orientation, the receiver-transmitter separation etc) that are expected in normal AEM surveys, variations that can influence the modelled subsurface conductivity structure.

The X and Z component TEMPEST data were initially screened using an automatic filter to remove negative values at late time caused by either IP effects or general late time noise. Manual processing was then undertaken, involving a visual inspection of results from the automatic processing as well as additional removal of noise where required.

3.2 Modelling and inversion

One of the primary objectives of reprocessing and inverting a part of the Coffin Bay TEMPEST survey was to map and interpret the spatial variations in the conductivity, particularly those associated with SWI interface. Although measured AEM data can be imaged by gridding the raw window/time channels, where early time channels normally are associated with near surface and later time channels with greater depths, this is not necessarily always the case. Raw measured data are as such not a direct representation of the depth, but rather of a slice in time. Although this kind of output can be useful for a quick overview of the distribution of more conductive vs more resistive areas, information about the distribution of conductivity with depth cannot be inferred. The measured AEM decay curves can, however, be converted through an inversion or transformation of the data to provide information about the conductivity distribution with depth.

The inversion of AEM data, and their presentation as maps or sections detailing a conductivity distribution in the subsurface is now commonplace. The representation of essentially continuous and gradational conductivity distributions as discrete conductive “units” or bounding layers is an effective way of summarising information from large AEM surveys. It enables users to visualise conductivity variations quickly and reliably in the subsurface in three dimensions (Lane 2000, 2002, Lane and Pracilio, 2000). To determine true conductivity variation with depth the data must be modelled. This entails taking data from each measurement point, sounding or fiducial along a flight line and estimating the parameters of a layered-earth, conductivity-depth model, which would produce the observed response. Figure 3-1 presents a graphical representation of the workflow used in deriving a model of the subsurface conductivity structure.

Accurate modelling of the subsurface conductivity also requires information about the characteristics of a specific system used, such as time gates, waveform, current, filters etc. as an inversion is an iterative process of minimising the misfit between forward modelled responses (using these system specifications) from an electrical earth model and the measured AEM response. The iterative process involving changing the parameters of the earth model until an acceptable misfit is obtained is a time-consuming part of the modelling. The result obtained from an inversion of AEM data is however not a unique result as several conductivity-depth models are able to fit the data within an acceptable range. This non-uniqueness emphasises the need for verifying the inversion results by independent information such as drill-hole data, down hole geophysical logs or other ground geophysical measurements.

Through the application of approximate transforms or layered inversions, conductivity values with depth can be calculated for each observation (sounding) made by the AEM system, and then stitched together into sections to provide a representation of the 2D variation of conductivity. This is sometimes referred to as a “para-section”. Further, the conductivity depth profiles can be combined into a 3D gridded volume from which arbitrary sections, horizontal depth slices (or interval conductivity images) and iso-surfaces can be derived. In this study, depth slices were extracted from the inversion results and then gridded as a 2D maps of conductivity for a given depth interval.

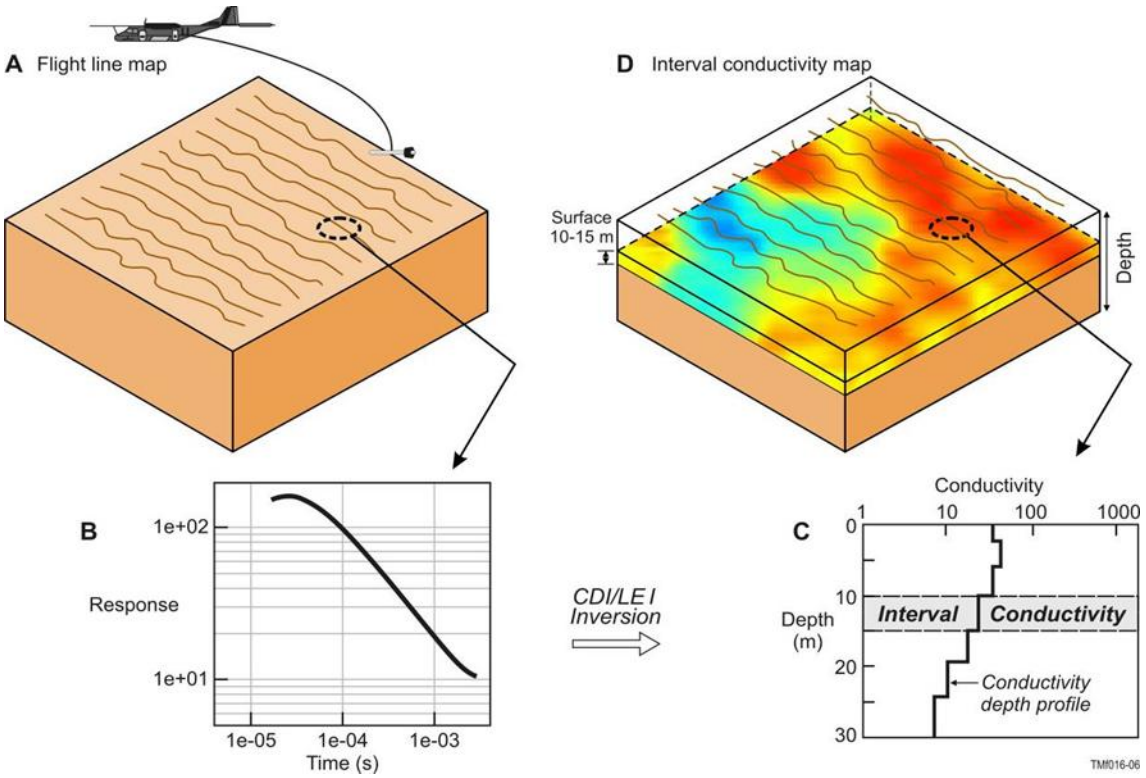


Figure 3-1: Schematic representation of TEMPEST fixed-wing time domain EM data acquisition and interpretation. A) Data are acquired along parallel flight lines, with data recorded at fixed time intervals (soundings) along each flight line; B) The EM receiver (housed in a "bird") towed behind and below the transmitter, measures the ground response as a function of time; C) The measured response is used to determine how conductivity structure varies with depth by transformation or inversion. Conductivity-depth values can be calculated for each observation, taking account of the elevation and geometry of the system above the ground; D) The modelled conductivity structure for each sounding can then gridded into conductivity-depth intervals to provide a spatial representation of the subsurface conductivity structure at different depths below the ground surface. These maps can be shown as elevations (mAHD) or as depth intervals below the ground surface ground surface; E) Individual soundings from a flight line or transect of several soundings may also be stitched together into conductivity-depth sections to provide a representation of the 2D variation of conductivity (a conductivity-depth section), sometimes referred to as a "para-section" (see also Figure 3-2).

3.2.1 Inversion model

The Coffin Bay TEMPEST AEM data were modelled using two different inversion methods. However, prior to inverting all lines, several approaches were considered and tested on a single line of data (line 10260). The results of this assessment are summarised in Figure 3-2. Consideration of a blocky (few) layer and smooth (many) layer conductivity model formed part of this assessment. Figure 3-2A shows the results from using a 5 layer 1D layered earth inversion (LEI), versus a sample-by-sample smooth model (30 layers) 1D LEI (Figure 3-2B). The black line running across the section indicates the model fit from the inversion, and models with low misfit between the modelled and measured response will be around 1 (as per axis on the right side of the section). Poor fits are observed on the left side of the section – possibly related to noise in proximity to the Coffin Bay town, and on either side of the resistive are between 4 and 6 kms along the section on the right side. This may indicate that the 1D assumption becomes invalid where the edges of a resistive basement are encountered. The smooth model (30 layer) inversions (Figure 3-2 B, C and D) yield similar model fits.

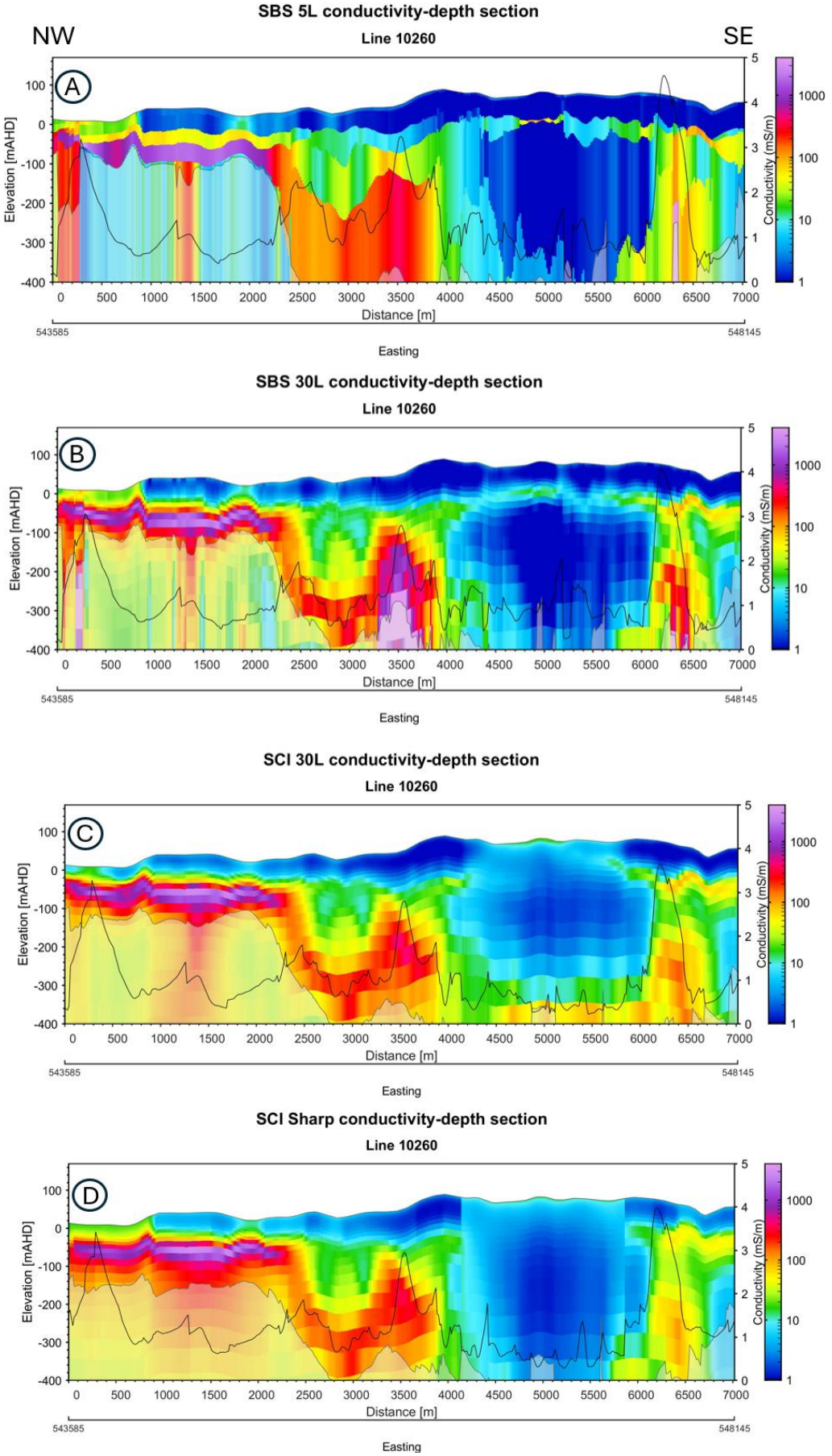


Figure 3-2: Conductivity-depth sections for different inversion approaches – Line 10260.

Two approaches were selected, following this review, specifically the smooth model 1D layered earth consisting of 30 layers with fixed thicknesses, and a sharp inversion, with a similar number of layers. Both a smooth layered model inversion and a sharp model inversion both containing 30 layers with first layer thickness of 1m and thicknesses logarithmically increasing down to 700m depth. A homogenous half space with a resistivity of 40ohmm was used for a starting model and both the X and the Z component data were used in the inversion. During the inversion there is an option to solve for layer parameters, transmitter altitude, receiver pitch and roll, tow cable length and receiver altitude (Figure 3-3), although the receiver pitch is by far the most important parameter to invert for (Auken et al. 2009), as the X-component and Z-component data are nearly uninterpretable if the forward response is not corrected for by the pitch of the bird.

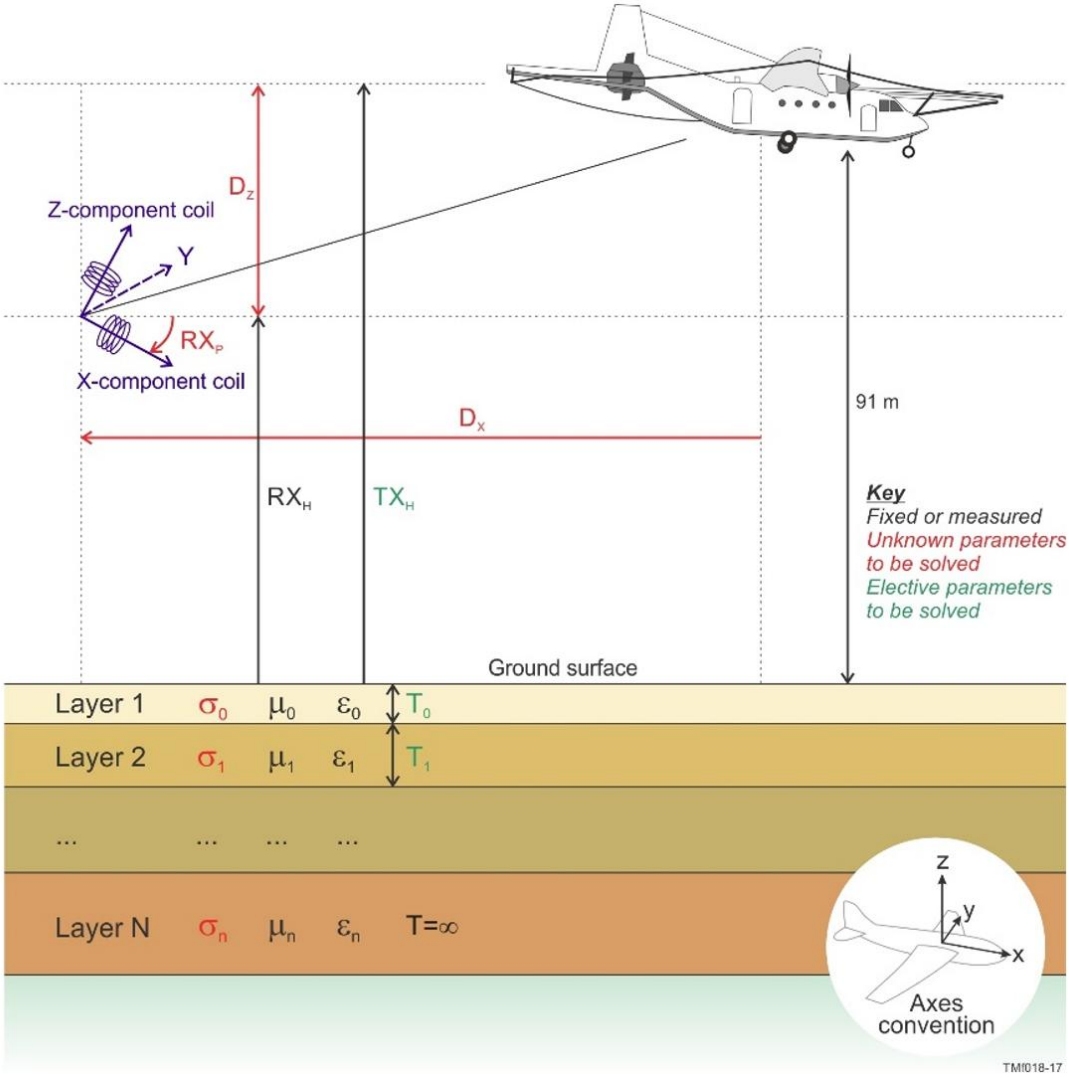


Figure 3-3: Schematic representation of parameters considered and solved for in the inversion

With the two types of inversions constraints can be applied to allow for varying degrees of change in conductivity of one layer to the next. The large number of layers and the gradual change in conductivity for the smooth type of model makes the resulting conductivity models appear continuous. While this can make it difficult to pick layer boundaries as these may appear rather diffuse, in this environment they are more likely to represent the change in conductivity with depth, including the diffuse region likely to be present at the top of the saltwater interface. To sharpen the definition of marked changes in conductivity, a sharp inversion was applied to the data with the intent of obtaining more pronounced layering (i.e. sharper layer boundaries).

Smooth Model Spatially Constrained Inversion (SCI)

The Coffin Bay TEMPEST survey was flown at a line spacing 400m which makes the spatially constrained inversion a potentially viable modelling choice for this dataset. The Spatially Constrained Inversion (SCI) methodology is described by (Viezzoli et al. 2008). The SCI is described as a quasi-3D inversion methodology, based on a 1D forward response, with 3D spatial constraints. The spatial constraints allow prior information (e.g., the expected geological variability of the area) to migrate along/through the entire dataset (Figure 3-2). The constraints for the SCI are set in a Delaunay triangulation, where the connection is made to the nearest, or adjacent sounding. The constraints in the Delaunay triangulation are given a weight according to distance, so that soundings closer together are more tightly constrained, whereas soundings far from each other are not linked at all. The output models balance the information present locally within the individual TEM soundings with the ones carried by the constraints, in this case from adjacent soundings. Conductivity models that honour information from along and across lines can result in a smoother appearance of the conductivity distribution as information is carried across from lines. The SCI has a demonstrated applicability in semi-layered geological settings as is expected in the Coffin Bay area.

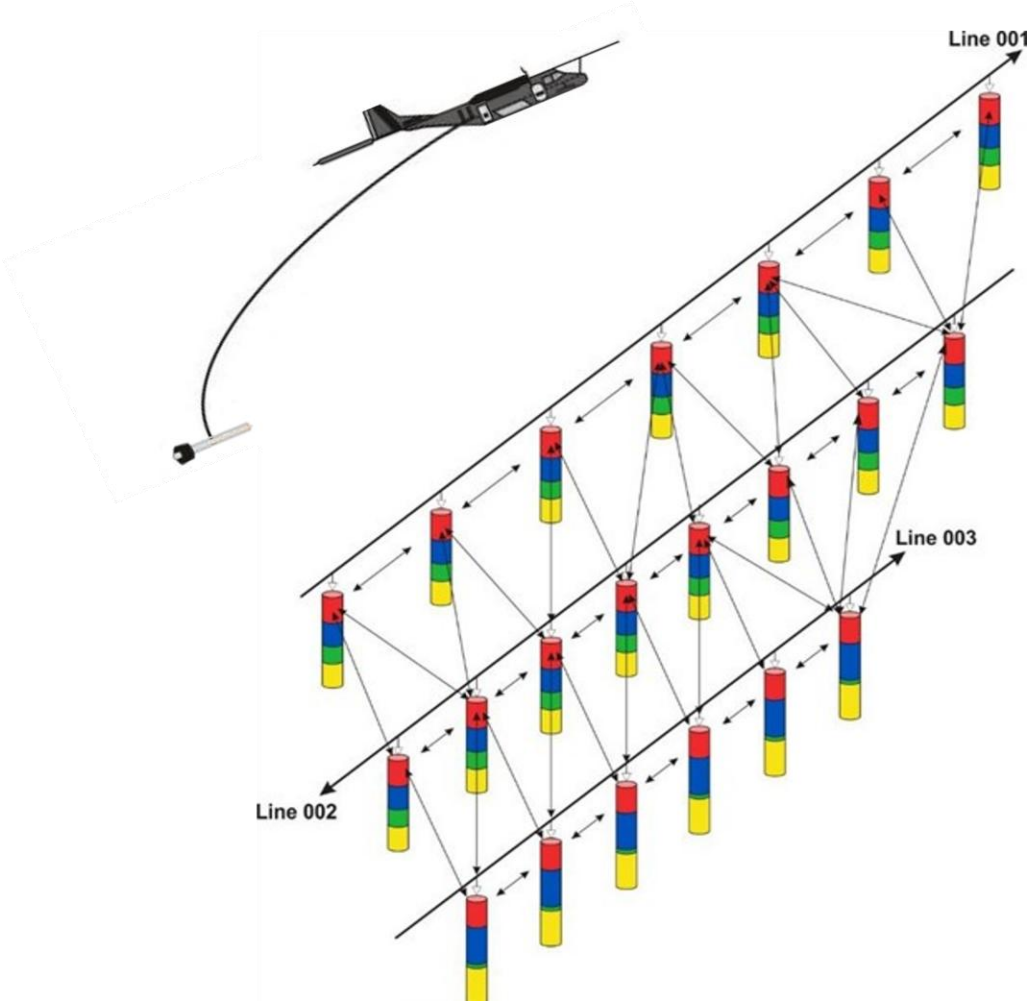


Figure 3-4: Schematic overview of the process of allowing prior information to migrate along and between a series of soundings (fiducials) acquired by an AEM system when they are inverted using the Spatially Constrained Inversion (SCI) procedure.

Sharp inversion

Traditional inversion options include an Occam style regularisation using smoothly varying 1D models with fixed vertical discretisation, producing very smooth models where layer boundaries are hard to recognise, and discrete few layer models with a fixed number of layers where the layer boundaries are allowed to

change in the inversion. The smooth layered model has shortcomings in terms of defining layer boundaries, but for the few layer model on the other hand it can be difficult to pick a number of a layers that will be valid throughout a whole survey, and as a consequence artefacts can be introduced in areas of unexpectedly complex geology.

The Sharp inversion methodology outlined in Vignoli et al. (2015) is a focussed regularisation technique which allows for an accurate reconstruction of resistivity distributions while maintaining the capability to reproduce or sharpen horizontal boundaries. The methodology promotes solutions that are compatible with the observed data and at the same time features a minimum number of spatial (vertical and lateral) model variations.

Depth of investigation

The presentation of conductivity models derived from AEM systems can be misleading if there is no attempt made to qualify the depth of investigation (DOI) of the measurement system. The depth of investigation is a complex quantity, being a function of the power, sensitivity and accuracy of the acquisition system, environmental noise levels (e.g. spheric and powerline sources), geologic complexity, the host conductivity and the target characteristics (e.g. a discrete object or an extensive layer, conductivity contrast to the surrounds) and the inversion procedure used (Lane 2000; Christiansen and Auken 2012). To ensure that the observed variations in measured conductivity reflect changing ground conditions, rather than inversion or model dependent changes arising from the inversion process, an estimate of the depth of investigation is calculated and presented on the conductivity-depth sections. This information assists the interpreter, helping to quickly evaluate the results and their validity. The DOI provides a depth to which the model is the most reliable, and model information below the DOI should be used with caution.

The DOI determination used here is based on the cumulative sensitivity of the actual model output from the inversion (it includes the full system response and geometry) and is described in Christiansen and Auken (2012). The data noise and the number of data points are integrated into the calculation, which is based on the final inversion model output and a recalculated sensitivity (Jacobian) matrix. In general terms the more conductive the ground, the ability to resolve deeper variations in conductivity (or the depth to which the inverted model is reliable) decreases. In more resistive ground, the system is able to resolve those variations more reliably to greater depths. The modelled conductivities in the survey area varies from being highly conductive over the sea resulting in a lower DOI, to being more resistive in the central parts of the survey where SWI is not present (Figure 3-3). Consequently, the modelled DOI is deeper.

The DOI varies significantly across the study region due to a dependence on the modelled conductivity structure, as well as noise levels and the signal strength. We found it to be approximately 50 mbgs (metres below ground surface) in the more conductive regions along the coast and generally 150–200 mbgs in the more resistive inland regions (Figure 3-3).

Elevation model

For this study we employed the SRTM 1sec DEM for the presentation of results (conductivity-depth intervals and sections).

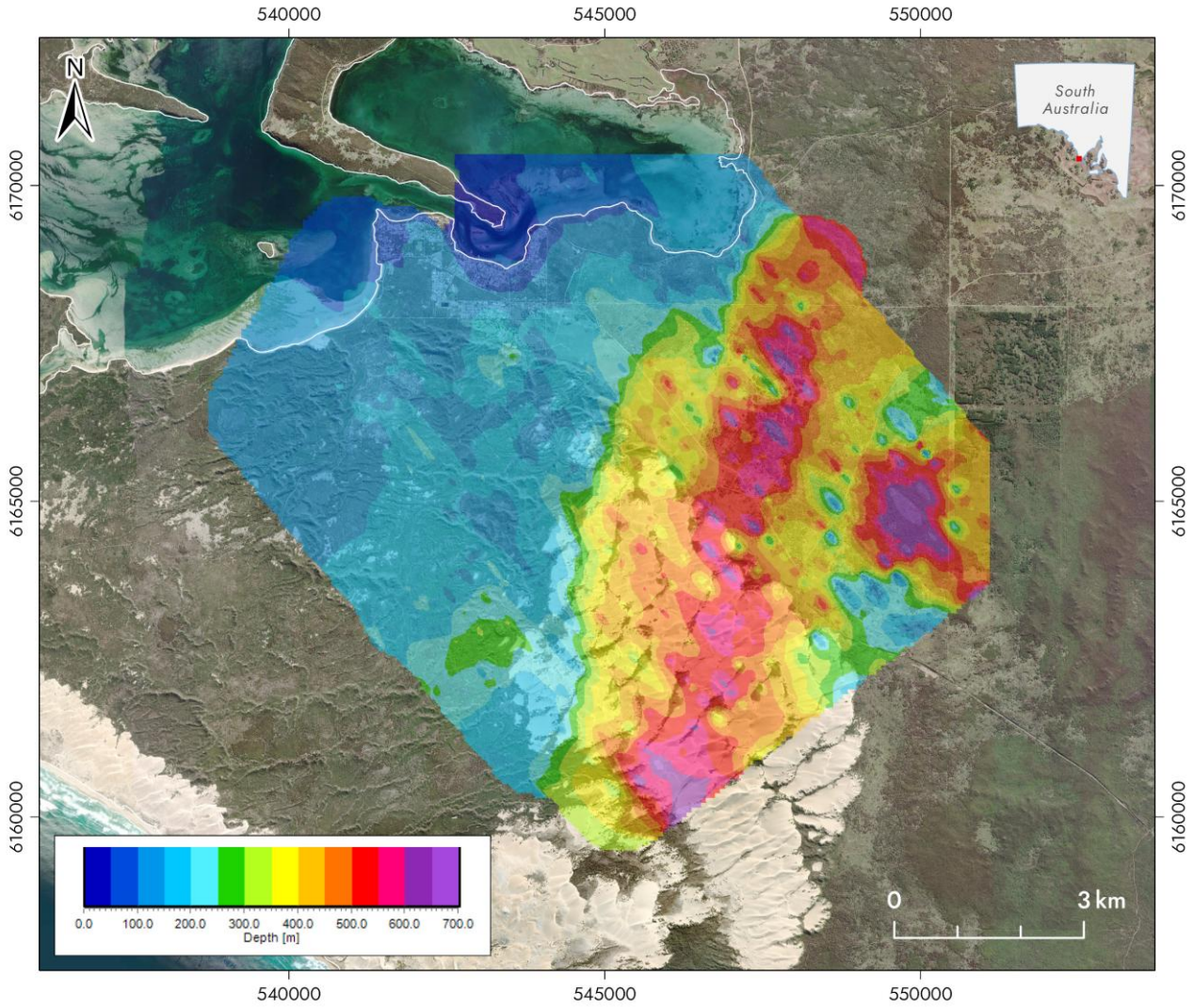


Figure 3-5: Gridded image of the Depth of Investigation (DOI) for the inverted lines of TEMPEST data.

4 Derived Products

4.1 Interval conductivities

Model outputs from the inversion of the Coffin Bay TEMPEST data include conductivity-depth *intervals* (expressed as "depth below the ground surface" or as elevation (mAHD)), and conductivity-depth *sections*, in this instance generated for each of the inverted flight lines which are numbered in Figure 2-4.

Examples of the two sets of interval conductivities (for the smooth model SCI) that were generated are shown in Figures 4-1 and 4-2, for "depth below ground surface" and "elevation" respectively. Both illustrate the ingress of salt water into the Quaternary aquifer, with an irregular saltwater interface extending several kilometers inland, but being laterally constrained by an unweathered Proterozoic basement. The AEM data suggest saltwater completely underlies a significant part of the fresh Coffin Bay A lens.

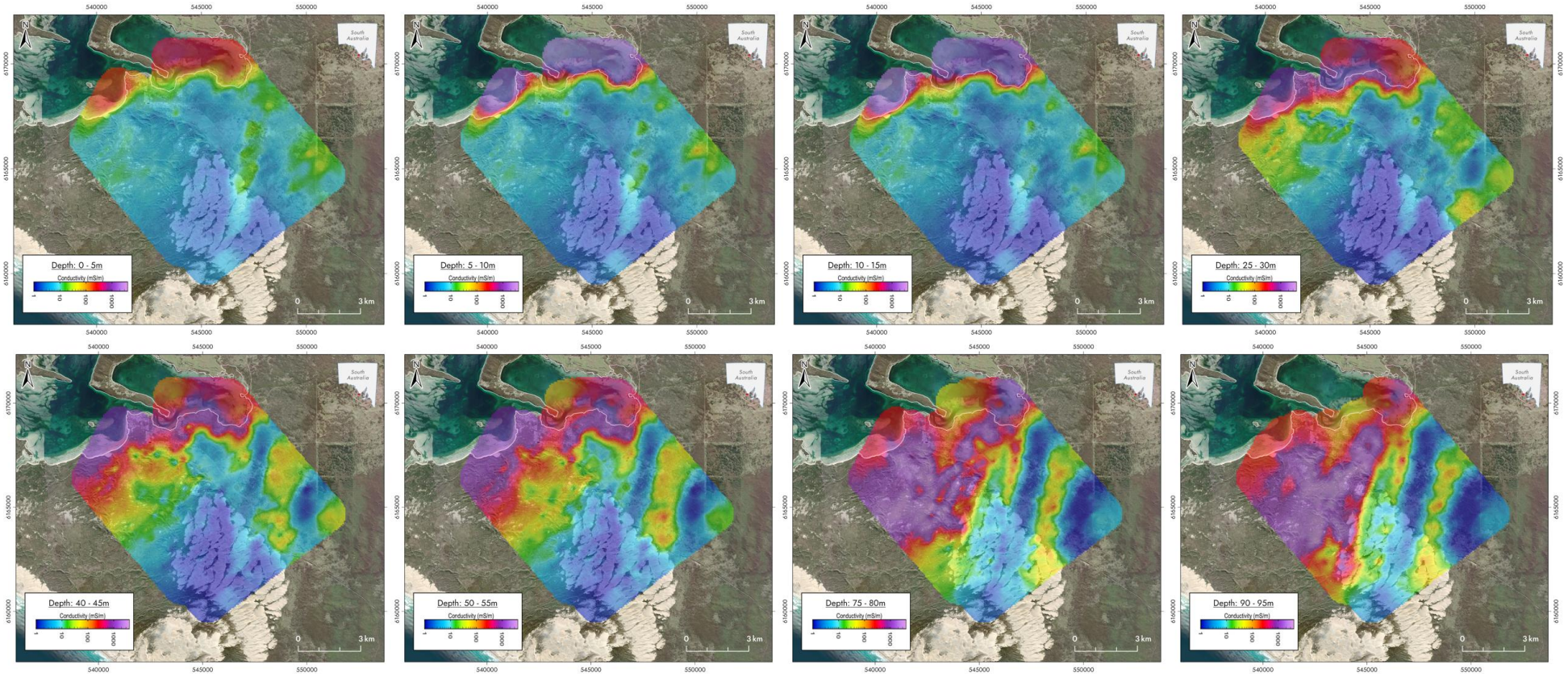


Figure 4-1: Example conductivity-depth intervals, for specified intervals (in metres) below the ground surface (BGS) overlain on true colour satellite imagery. The top row shows a sequence of depth intervals starting at 0-5m BGS, increasing in depth to 25-30m BGS. The lower row shows depth intervals at greater depths. Evidence of the saltwater interface progressing inland (represented by elevated conductivities) becomes clear in the 25 to 30m depth interval, with the irregularity of its landward shape becoming more apparent at greater depths. The influence of the unweathered Proterozoic basement (represented by elongate NNE-SSW resistive zones) on the geometry of the SWI and its extent inland is apparent in the deeper interval conductivities. Irregularities in the SWI, as it extends inland, may reflect lateral changes in the lithology of the Quaternary, underlying sediments and the Proterozoic basement.

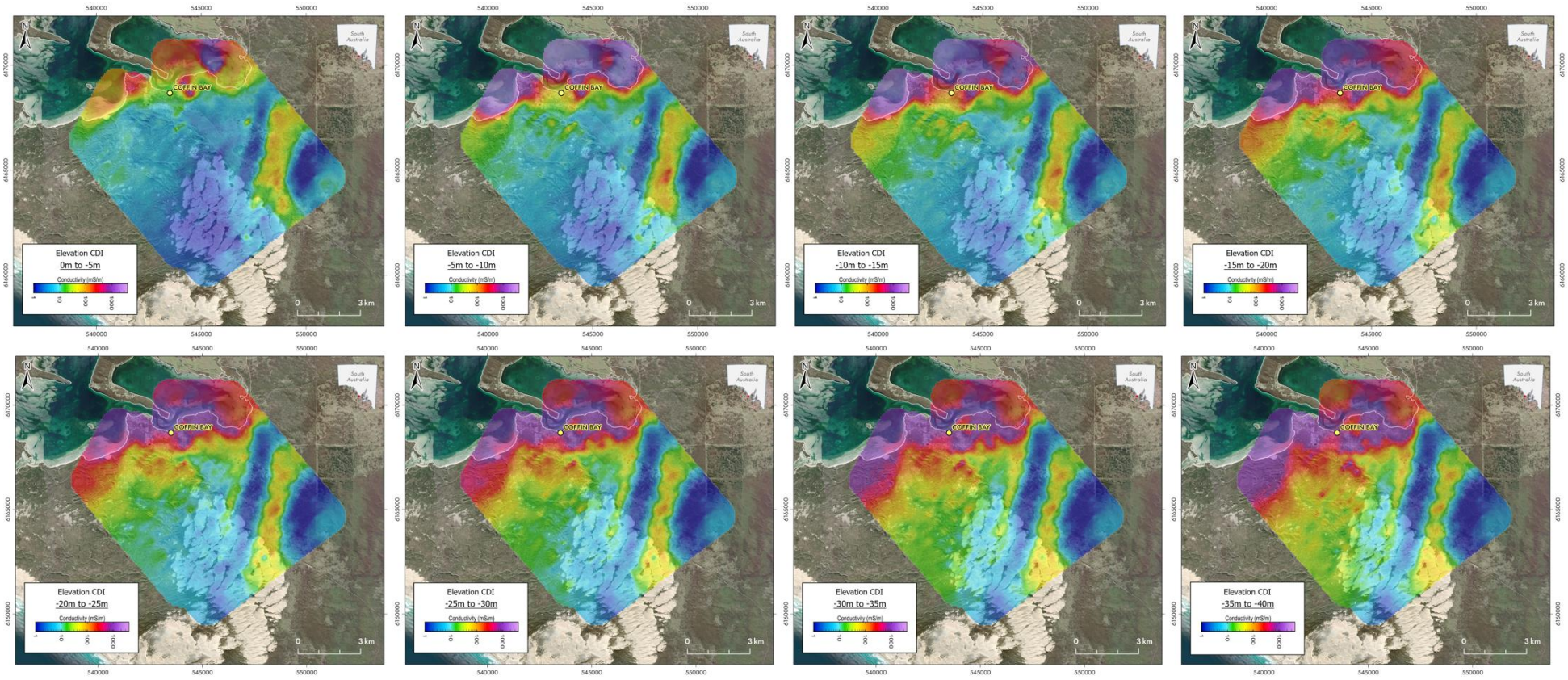


Figure 4-2: Example conductivity-depth intervals for elevations in metres Australian Height Datum (mAHD), for specified intervals overlain on true colour satellite imagery. The top row shows a sequence of depth intervals starting at 0 mAHD, and incrementing in 5 metre intervals to 20 mAHD. The lower row of images extends the depth shown to -40 mAHD. The SWI, defined by elevated conductivities (yellows, reds and purples) is shown to extend inland from the coast and is limited in its eastward extent by a resistive (blue) basement high which strikes NNE – SSW on the eastern side of the inverted data set.

4.2 Conductivity-depth sections

Conductivity sections for each of the inverted flghtlines (see Figure 2-4) were also produced as illustrated in Figure4-3 and 4-4 for a smooth model (30 layer) SCI, and a 30 Layer sharp SCI respectively. Sections for each of the inverted flightlines are reproduced in the Appendices (Appendix A.1.2).

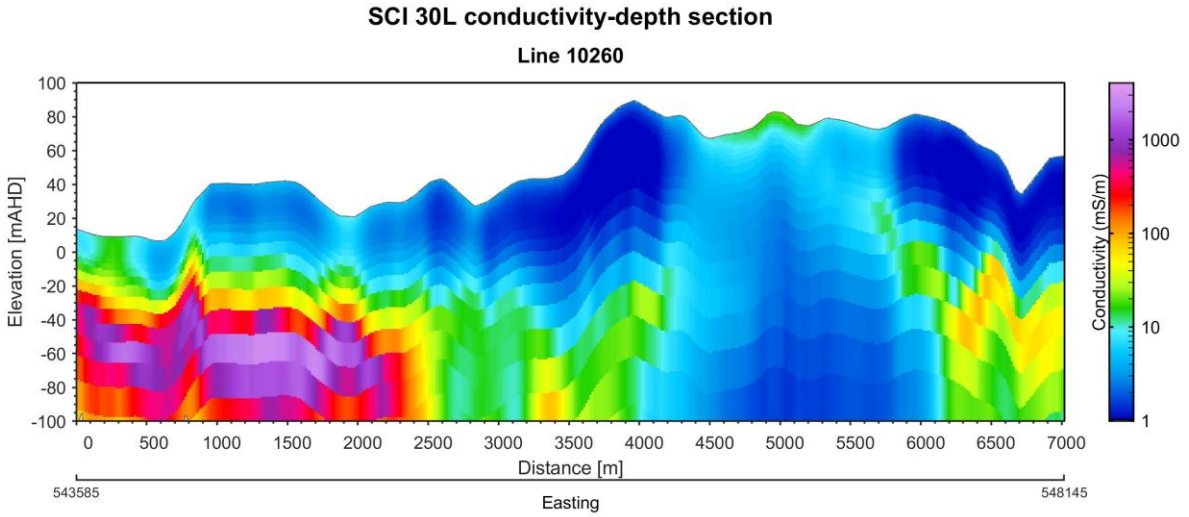


Figure 4-3: Conductivity-depth section for a 30 Layer, smooth SCI for Line 10260. The section is 7km long, oriented with the NW on the left. It shows a highly conductive, laterally extensive, and sub-horizontal zone on the left side of the section which is attributed to saltwater ingress into the Quaternary aquifer from the coast. The topography on the section is defined by the SRTM 1sec data. Disruption of the more conductive layers between 4000 and 6000m is attributed to the presence of an unweathered basement ridge extending into the plane of section.

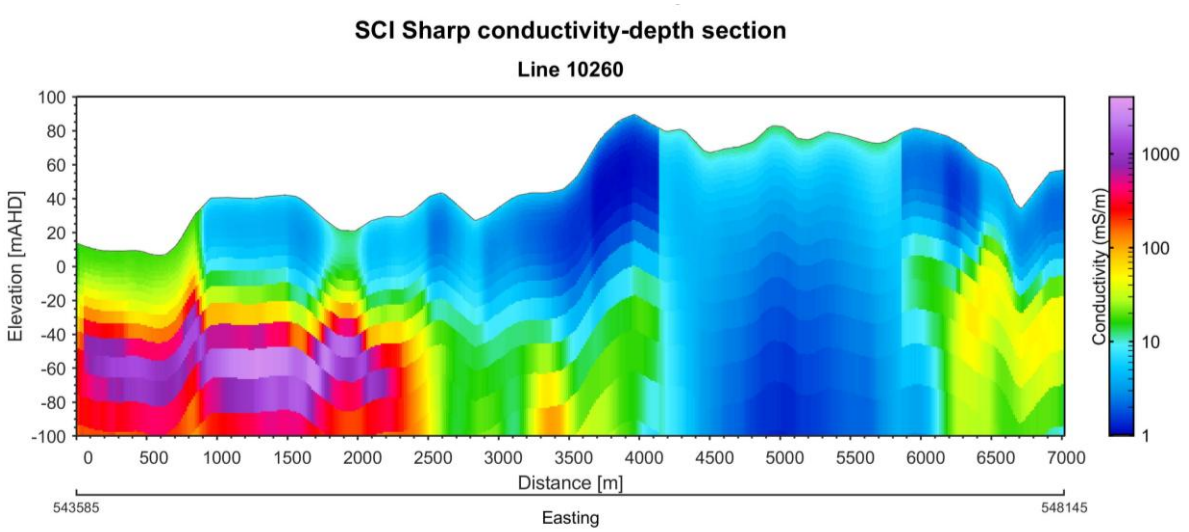


Figure 4-4: Conductivity-depth section for a 30 Layer, sharp SCI for Line 10260

The modelled conductivity structure was compared with borehole logging (inductive conductivity) data, for two bores, acquired by DEW (data courtesy Kent Inverarity (DEW)). The inductive conductivity logs were acquired on the 31/10/2024. The locations of the two bores sampled are shown in Figure 4-5, along with profiles from the inductive conductivity logging and the results of the inverted TEMPEST data for two fiducials closest to the bore locations. Variations in the borehole induction logs between 0 and 50m below the ground surface may relate to changes in lithology in the Quaternary aquifer. These are fine scale changes that cannot be modelled by the AEM data set. Rather the AEM models define a gradual increase in conductivity, peaking

around 60m below the ground surface. The inductive logs also trend towards this peak. It is worth noting that the borehole logs are sampling the subsurface conductivity a few metres from the bore, whereas the TEMPEST sounding represents the modelled response from an area several hundred metres in diameter. Similarities between the two data sets provides confidence that AEM modelling is representing the ground conductivity structure, albeit at a coarser scale.

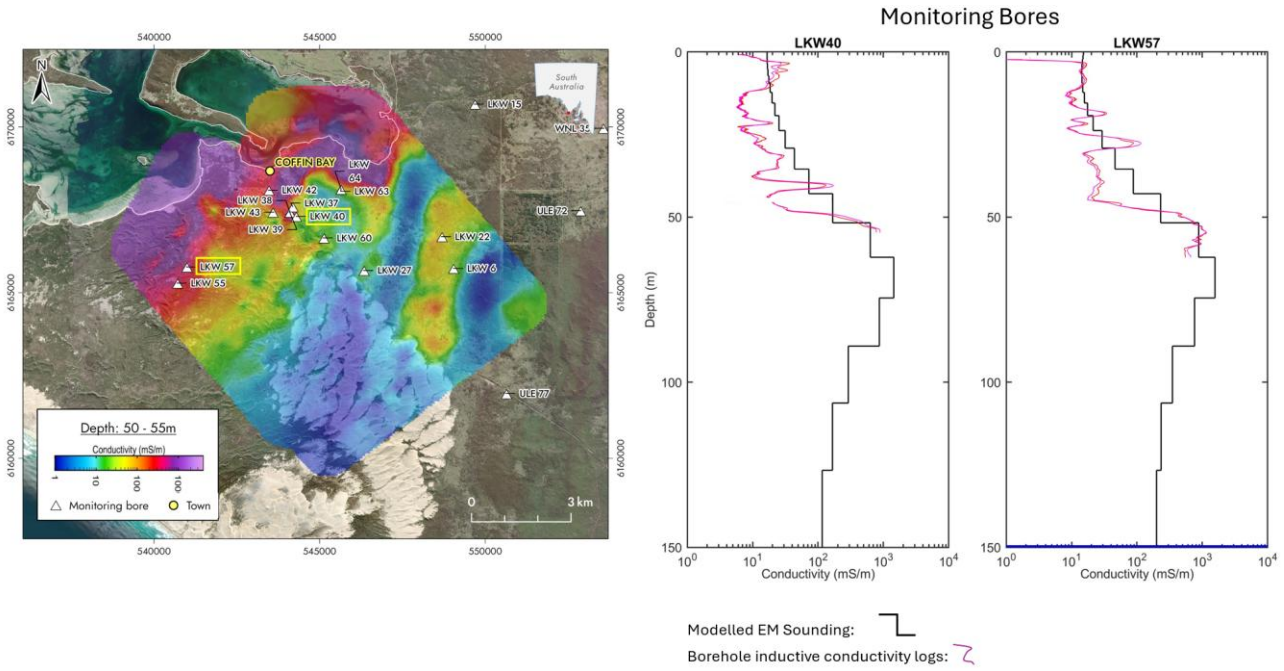


Figure 4-5: A pseudo coloured conductivity-depth interval for 50-55m (BGS) overlain on a satellite image with monitoring bore locations (left panel), with inverted (Sharp model SCI inversion) soundings (right panels) from the TEMPEST data closest to bores LKW40 and LKW 57 (locations indicated on accompanying image). The results of the recently acquired borehole inductive conductivity logs (medium and deep induction are overlain on the TEMEPST models (left panels).

4.3 Saltwater Interface

Results from the inversion of the TEMPEST data indicated that they could be used to address the primary objective of the study; namely to define the geometry of the saltwater interface including its upper surface.

The conductivity-depth sections (see Appendix A1.1) show a highly conductive subsurface unit, interpreted to be the saltwater interface, propagating eastwards from the near surface at the coast, inland to depth with its eastwards extent sharply constrained by a resistive NNE-SSW feature (See, Figure 4-6). This is associated with a faulted magnetic basement high (see Figure 14 in Fitzpatrick et al. 2009), overlain by a thin sequence of Cenozoic sediments including the Quaternary Bridgewater Formation. The conductivity models also suggest that saline groundwater appears to propagate between basement highs, as suggested in Figure 4-6, which indicates a N-S conductive finger linking the coast and LKW27.

A key output from the study was to generate a model of the elevation of the upper surface of the SWI. This was achieved using a three- step approach with the first requiring the definition of an interface conductivity cut-off value (representing the top of the SWI), which is then followed by the computer picking the cut-off value for all points along a flight line (see Figure 4-7). This process is undertaken for all flightlines, and elevation of the picked boundary is then gridded.

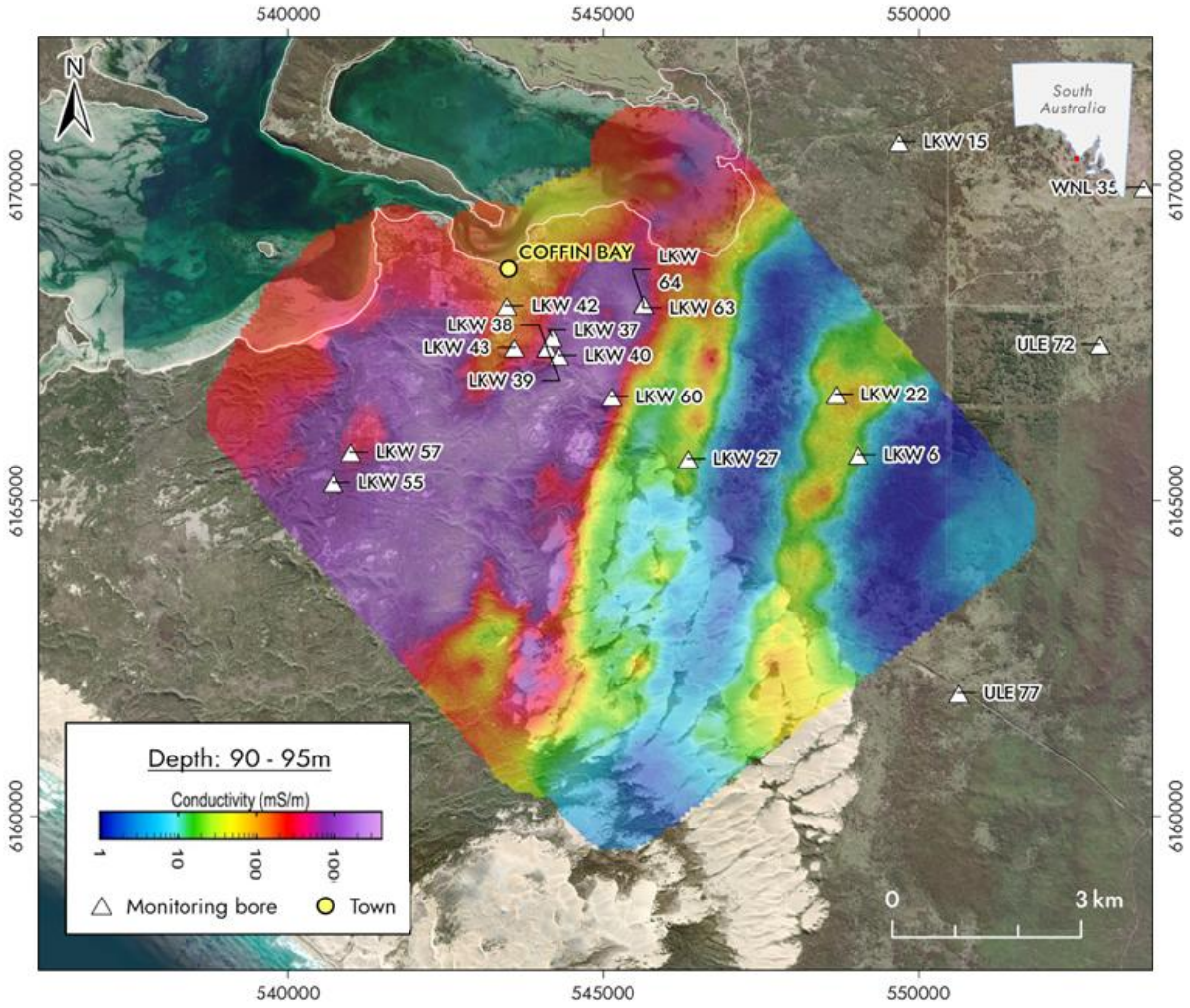


Figure 4-6: Interval conductivity image for depths of 90-95m below the ground surface, showing the sharp boundary between the conductive, saline groundwater to the west and a resistive (basement) unit to the east. The sharp boundary extends south from bore LKW63 to LKW60 and southwards from there.

A "conservative" cut-off value, specifically 1000mS/m, was identified which facilitated the generation of a spatially continuous interface. Higher cut-off values were tested, but they produced irregular surfaces that made interpretation more difficult.

A model for the elevation of the upper surface of the SWI is shown in Figure 4-8. It indicates that the top of the SWI dips to the south-east, being close to sea level at the coast, decreasing to > -70m AHD where the basement is interpreted to terminate its southeastern extent. The model also indicates significant irregularity of the interface. Examination of the elevation surface suggested that the saltwater interface peaks directly beneath, and adjacent to the Coffin Bay Town Water supply bore field (see Figure 4-9). This is also borne out in the modelled conductivity-depth section for line 10260 (Figure 4-10).

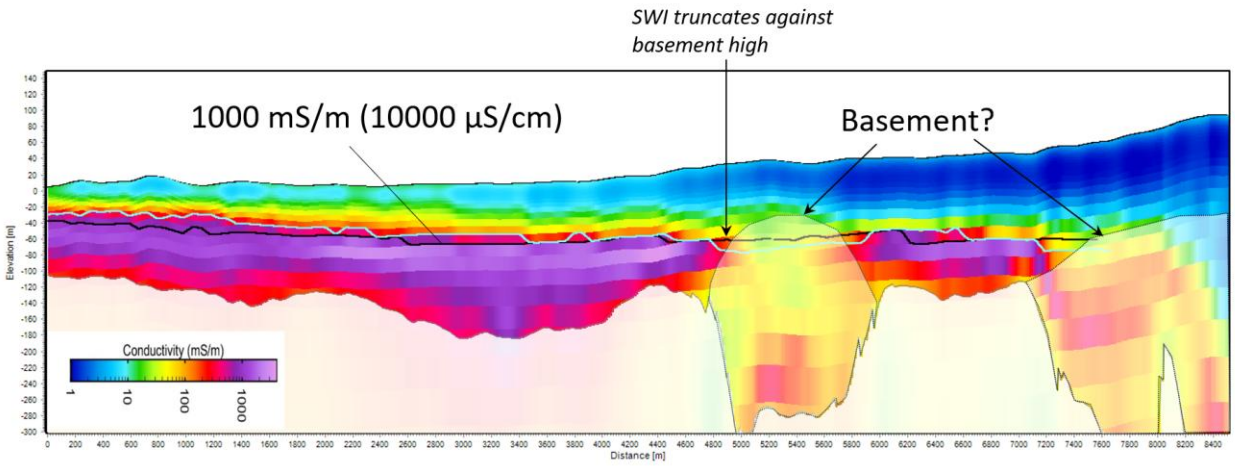


Figure 4-7: Picked interface lines for different cut-off values for a single flight line (line 10220). Note that the elevation of the SWI decreases inland as is expected and truncates against an interpreted basement high.

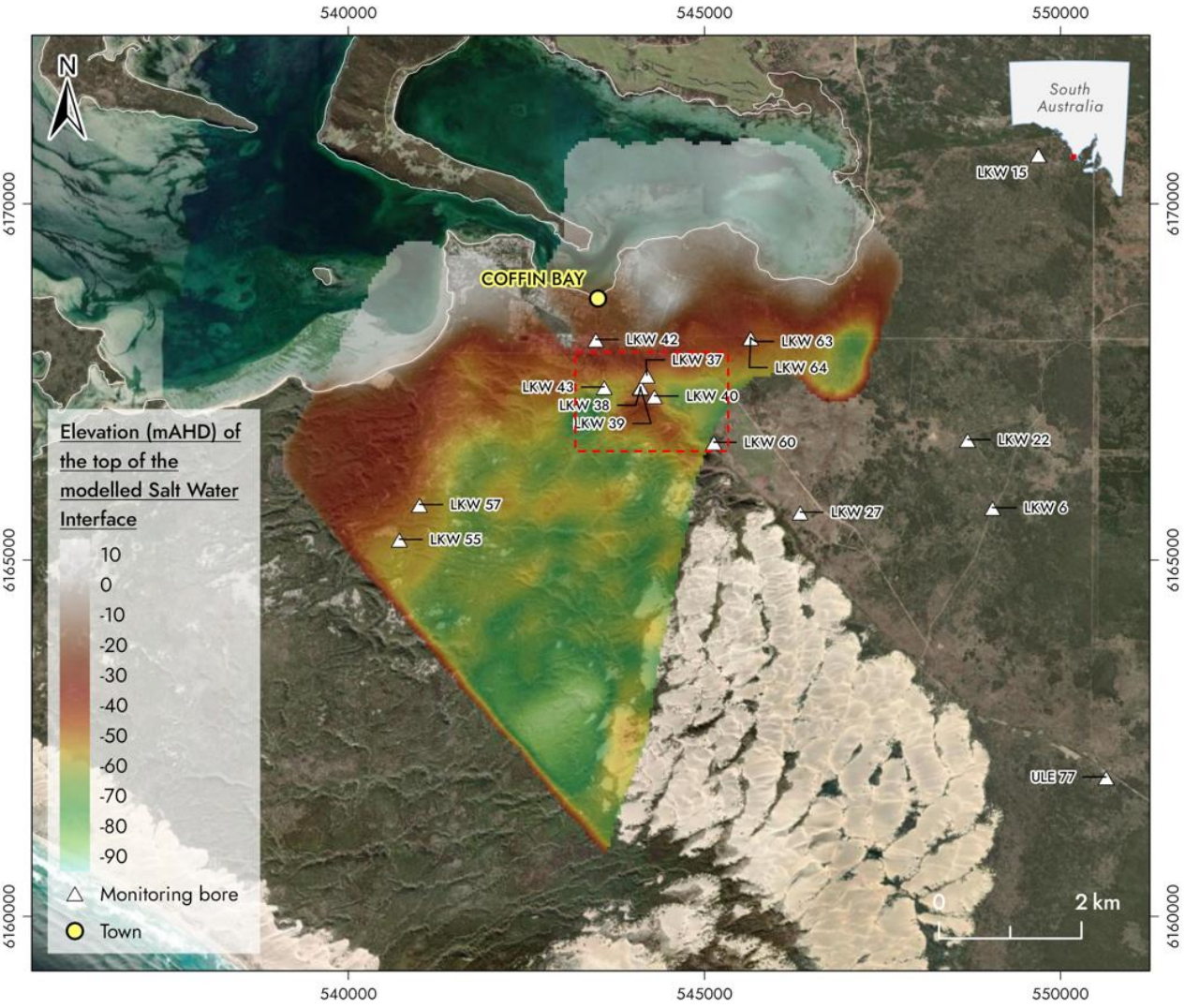


Figure 4-8: Model of the elevation (mAHD) of the *top* of the saltwater interface derived from inverted TEMPEST data for the area inland of Coffin Bay township. The pseudo-coloured image of elevation is overlain on a Satellite image of the area. Monitoring bore locations are also detailed. The area delimited by the red dashed rectangle is reproduced in Figure 4-9. The elevation of the SWI decreases inland from the coast, and the southeastern extent is defined by the truncation of the SWI against a NNE-SSW oriented basement high.

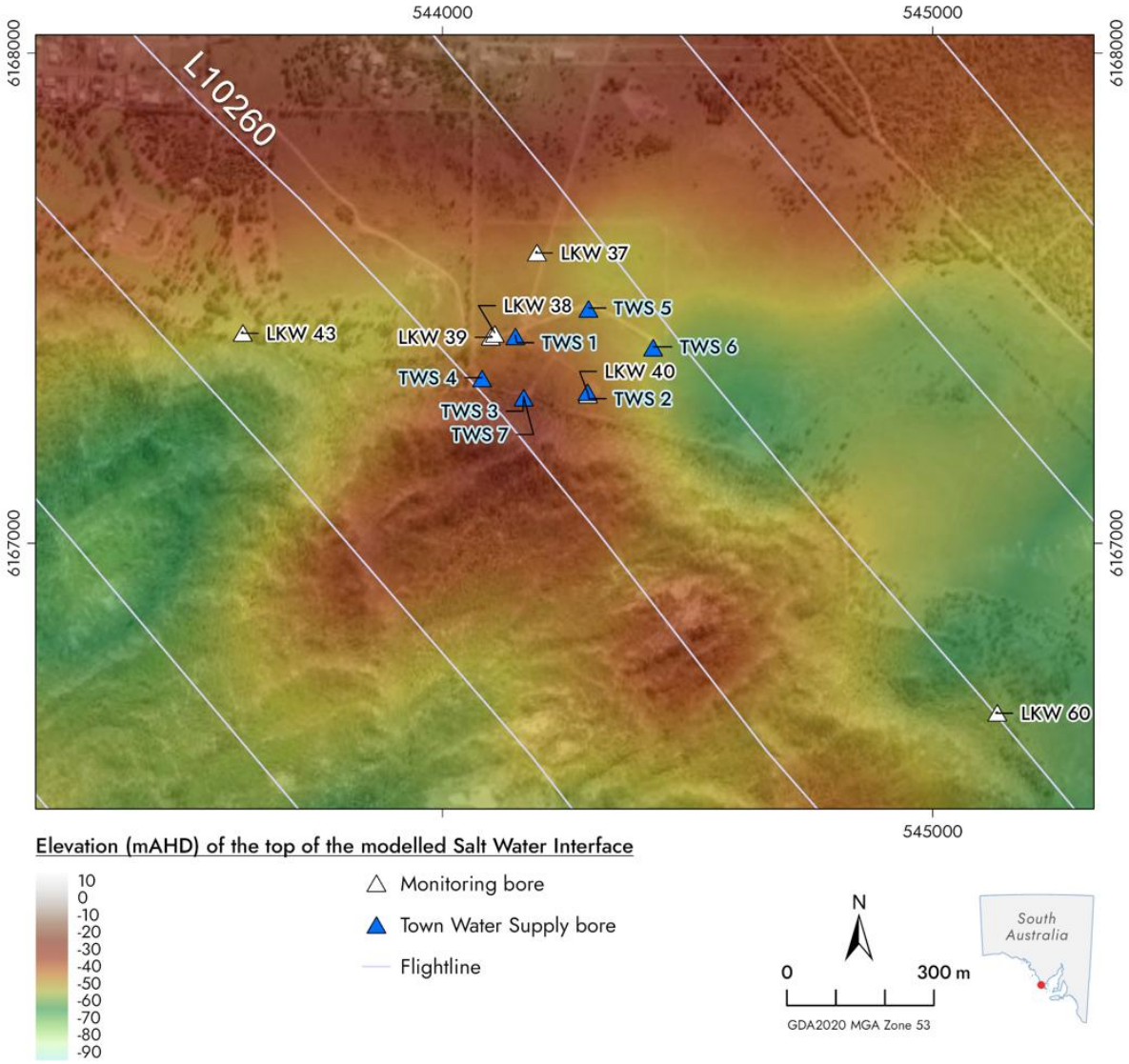


Figure 4-9: Pseudo coloured model of the elevation of the upper surface of saltwater interface extending through the Quaternary aquifer beneath the Coffin Bay town water supply bore field. TEMPEST AEM flight lines are overlain, with line 10260 labelled. This line intersects the SE margin of the bore field.

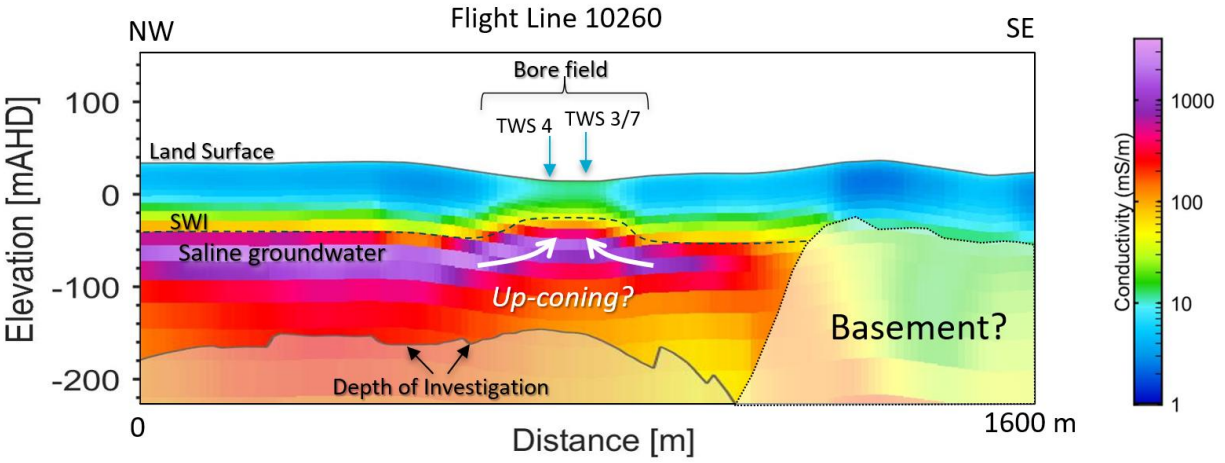


Figure 4-10: Conductivity-depth section for a subset of flightline 10260 which transects the southwestern margin of the Coffin Bay town water supply bore field. The section covers the extent of the line shown in Figure 4-8. The relatively abrupt termination of the laterally continuous conductive feature to the southeast of the bore field strongly suggests that the interface terminates against a basement high in the southeast.

Whether this is a function of saline up-coning through groundwater pumping, as illustrated in Figure 4-10 and conceptually in Figure 4-11, is not clear. Ward et al (2009) note that saltwater up-coning occurs below the point of extraction; but that the speed and severity is linked to the thickness of freshwater between the bottom of the production zone and the freshwater-saltwater interface.

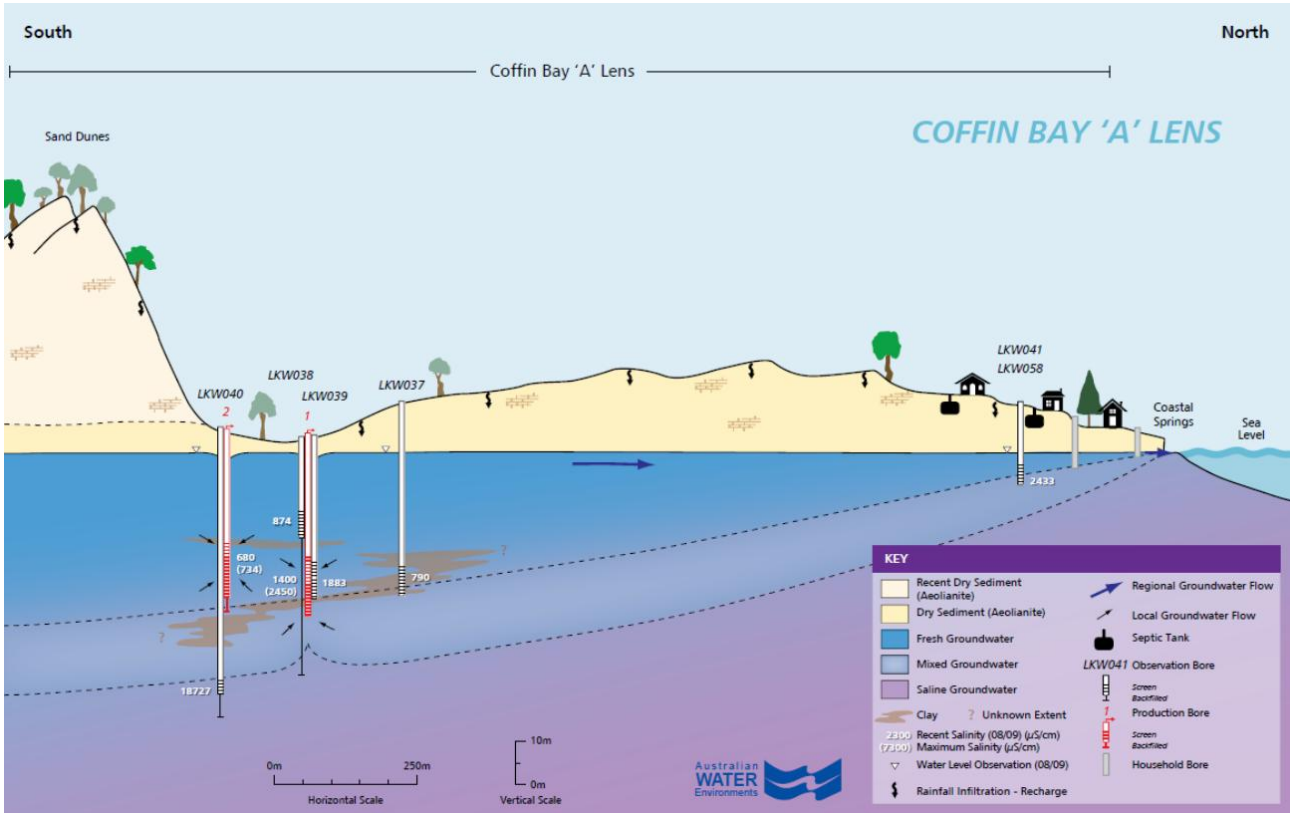


Figure 4-11: Conceptualisation of the Coffin Bay A lens fresh and saline groundwater interactions, illustrating the potential for saline up-coning. Figure sourced from Ward et al. (2009).

Consideration of the vertical conductivity structure around the Coffin Bay town water supply bore field suggests that there may be some lateral connectivity with the saline groundwater system at depth and that the postulated up-coning may be further complicated by the possible influence of heterogeneity in the aquifer properties (hydraulic properties and recharge). These may be linked to spatial variations in lithology. Figures 4-12 to 4-17 illustrate spatial changes in the subsurface conductivity structure around the town water supply and possible lateral connections of the SWI and the zone of suggested up-coning beneath the bore field at depth.

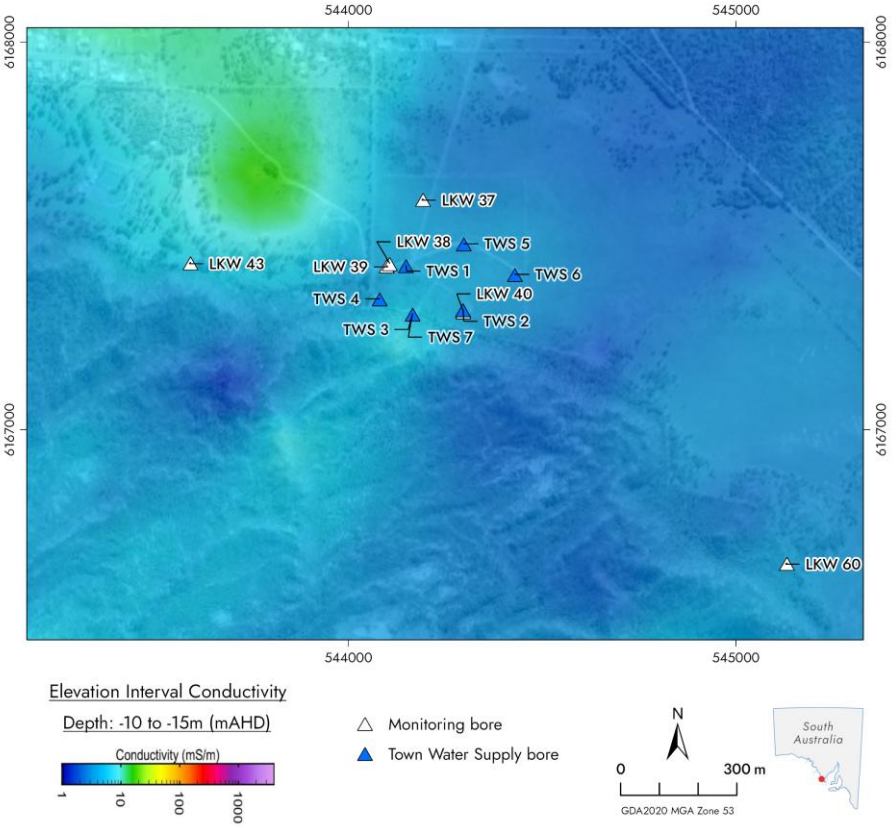


Figure 4-12: Elevation interval conductivity -10 to -15 mAHD

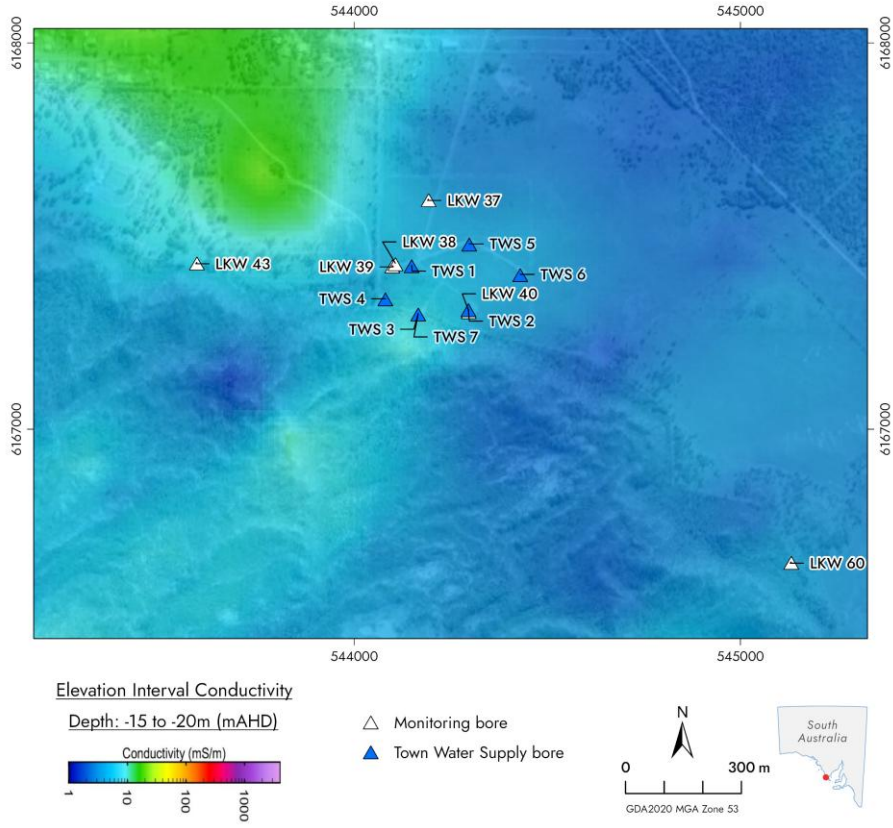


Figure 4-13: Elevation interval conductivity -15 to -20 mAHD

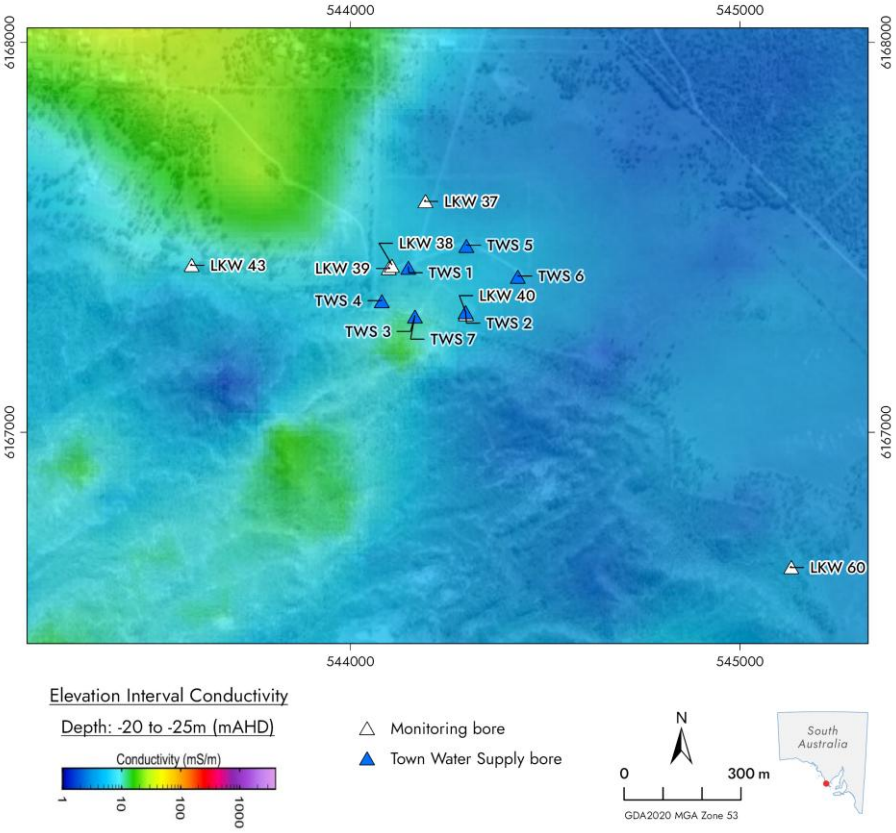


Figure 4-14: Elevation interval conductivity -20 to -25 mAHD

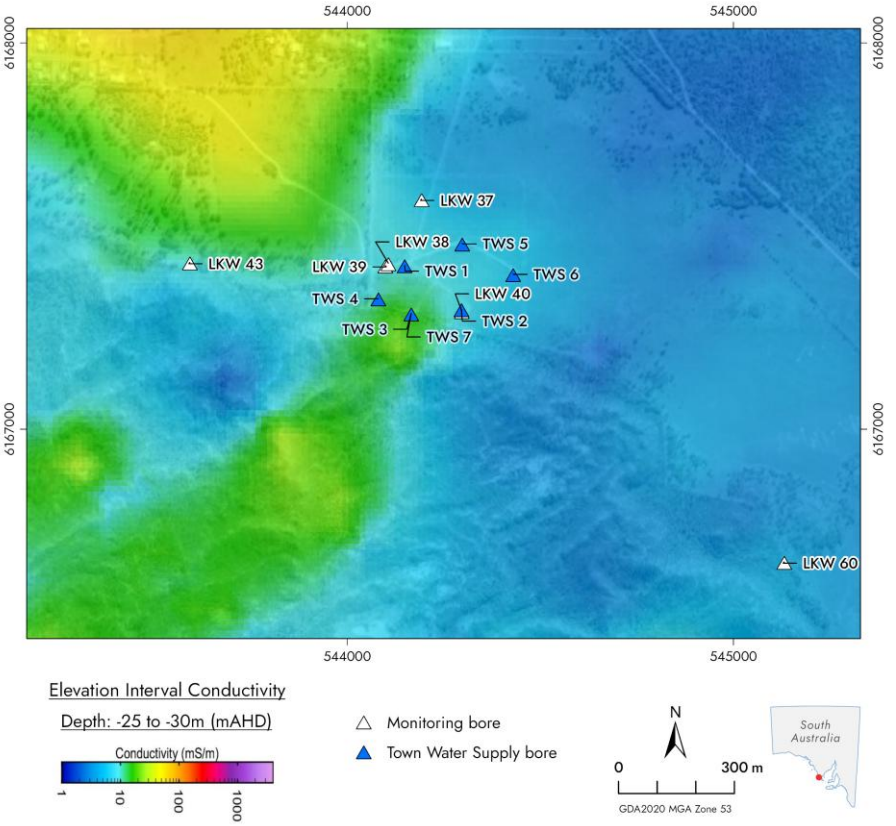


Figure 4-15: Elevation interval conductivity -25 to -30 mAHD

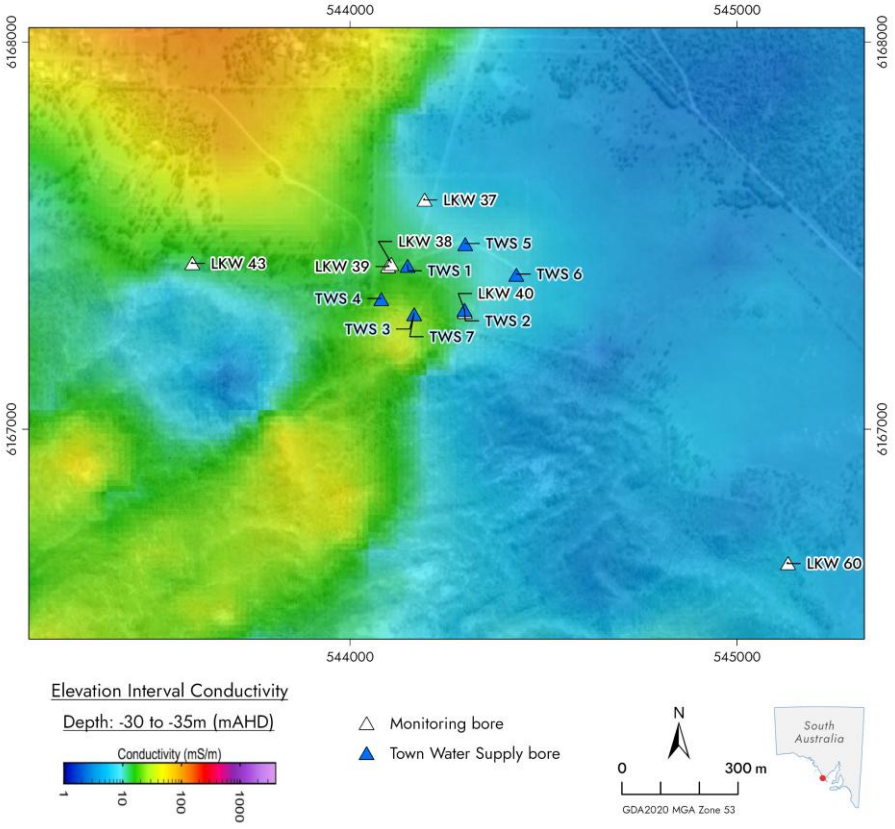


Figure 4-16: Elevation interval conductivity -30 to -35 mAHD

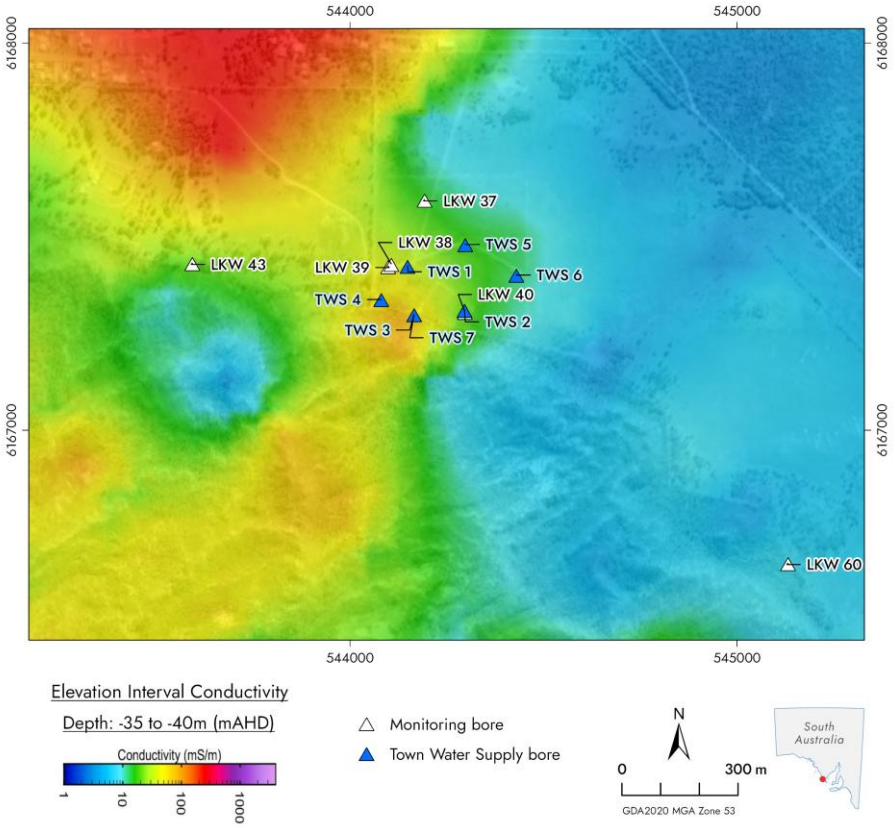


Figure 4-17: Elevation interval conductivity -35 to -40 mAHD

5 Summary

1. A spatially constrained smooth model 1D layered Earth inversion on a subset of an historical fixed-wing time-domain AEM data set (TEMPEST) covering the Coffin Bay area, including the Coffin Bay A lens system, was undertaken to refine a model of the subsurface conductivity structure associated with saltwater intrusion.
2. The modelled AEM data accord with independently measured borehole inductive conductivity data, with elevated conductivity coinciding with a spike in the borehole conductivity data and sonde measurements. This is attributed to saltwater ingress into the Quaternary aquifer.
3. Model results from the AEM inversion indicate that the saltwater intrusion extends from the coast, several kilometers inland into the Quaternary aquifer, and it is truncated on its eastern margin by unweathered Proterozoic basement rocks which strike NNW-SSE.
4. The intrusion is characterised by a variable geometry which may reflect variations in the hydraulic properties of the sedimentary aquifer. Linked to this is a suggestion that spatial variations in the lithology of the Quaternary aquifer may play a role in saltwater ingress.
5. The morphology and elevation of the upper part of the saltwater interface, as defined from the inverted AEM data, shows significant variability.
6. The modelled conductivity structure in the AEM data suggests that the saltwater interface rises beneath the town water supply bore field and in surrounding areas, which may be due to up-coning of the SWI linked to pumping. The elevation change for the SW interface in the area under the town water supply bores is >30m compared with modelled elevations to the NE and S.

6 Recommendations

Given the suggest complexity from the modelled SWI, coupled with the relatively broad scales of data acquisition the following recommendations might be considered:

1. A surface ground geophysical investigation be conducted using time-domain electromagnetic instrumentation to reaffirm the results of the AEM modelling, and to confirm suggestions of up-coning in the vicinity of the town water supply bore field. This need only comprise of several transects oriented to cross the suggested zone of up-coning identified in the AEM data. The higher resolution of a ground survey coupled with a constrained inversion of the acquired data may provide a more accurate estimate of the depth to the SWI beneath the production bores. The suggested transects for ground follow-up are summarised in Figure 6-1. The companying table (Table 6-1) details the purpose of the proposed transect.

Table 6-1 Proposed ground time domain EM transects

Transect	Target	Length (approx.)
1	More detailed definition of geometry of the elevation of the SWI beneath Production bores	450m
2	More detailed definition of geometry of the elevation of the SWI beneath Production bores and elevation beneath adjoining dune system	500m

3	Geometry of SWI progressing from coast progressing inland to TWS	900m
4	Transect from lower elevations of the modelled SWI across the area of suggested "up-coning"	1600m

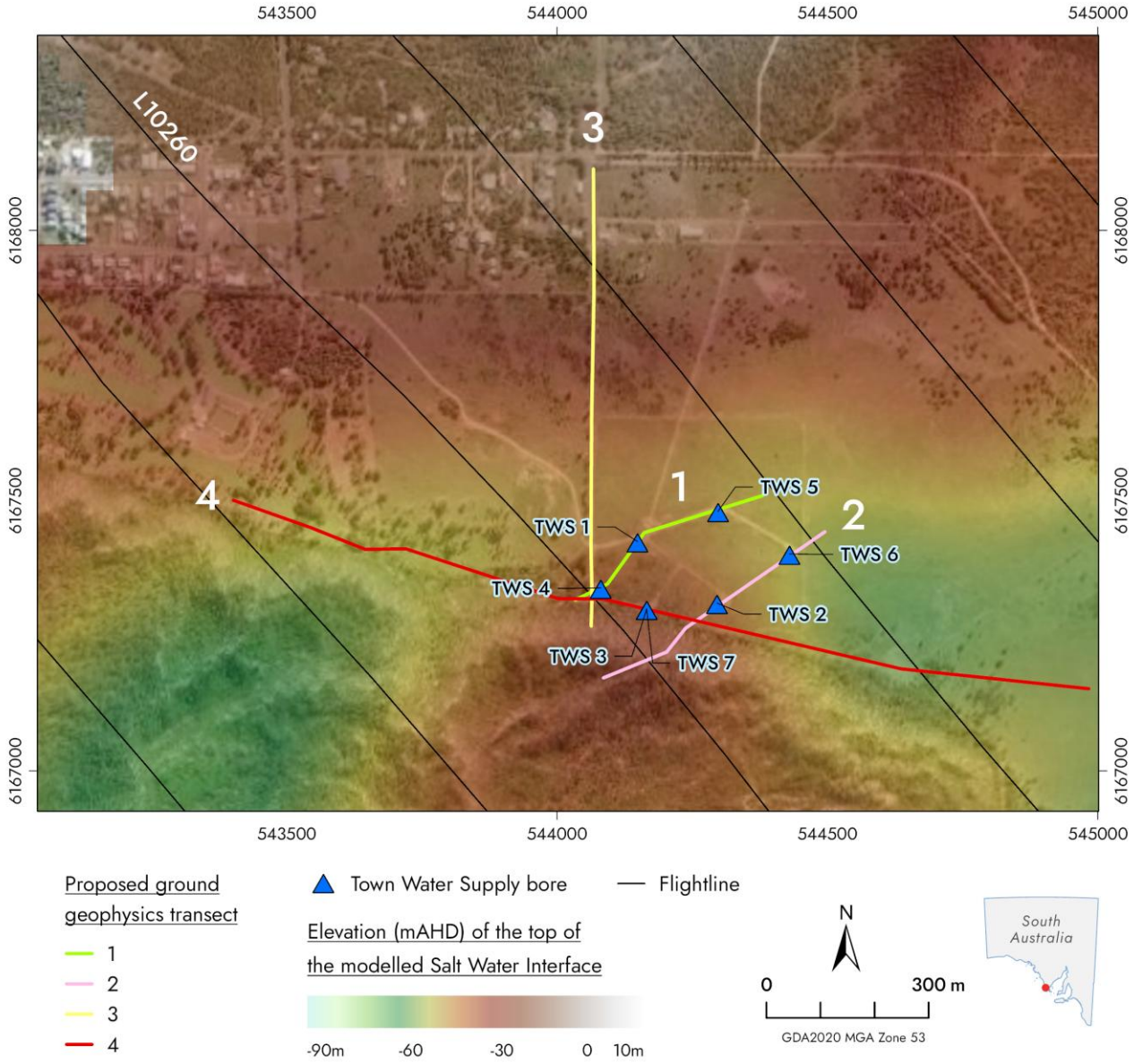


Figure 6-1: Proposed orientation and length of ground EM transects for the Coffin Bay town water supply bore field. Transects are plotted on a map of the elevation of the modelled saltwater interface.

Previous studies of the Coffin Bay Lens system (Clark et al. 2003) suggested that the use of surface geophysical methods may be challenged by the vegetation of the area, particularly in the dunes to the south-east of the town, but new technologies such as the STEMProfiler (see Maurya et al. 2024) may alleviate these.

2. Further work is required to assess the risk of up-coning linked to bore distribution, bore depth, pumping rates and persistence in Coffin Bay A lens, particularly if increased extraction rates are being considered.

3. Linked to point 2 above, additional ground EM transects should be considered to the SE (towards LKW60 and LKW 27) of the existing town water supply bore field, to confirm whether options to supplement the town water supply might exist in that area.

4. Closer examination of available lithological and geophysical logs from the monitoring and water supply bores may be warranted to help explain the variable character of the SWI. One of the data gaps noted for the area from previous studies (see Ward et al 2009), was the definition of aquifer properties (especially hydraulic conductivity and recharge) in the coastal fringe area, and the possible influence of heterogeneity in both properties on the SWI. Potentially surface and borehole nuclear magnetic resonance (NMR) surveys may assist in addressing this.

7 References

Annetts, D, Ibrahimi, T, Davis, A, George, R, Cahill, K, Munday T and Paul R. (2015) The application of AEM to mapping sea-water intrusion at La Grange, WA, ASEG Extended Abstracts, 2015:1, 1-4, https://doi.org/10.1071/ASEG2015ab164

Auken, E, Christiansen, AV, Viezzoli, A, Fitzpatrick, A, Cahill, K, Munday T and Berens, V (2009) Investigation on the groundwater resources of the south eyre peninsula, South Australia, Determined from Laterally Constrained Inversion of Tempest Data., ASEG Extended Abstracts, 2009:1, 1-5, DOI: 10.1071/ASEG2009ab121

Clarke, DS, Berens, V, and Dennis, KJ (2003). Uley South – Coffin Bay Observation Well Network Review. South Australia. Department of Water, Land and Biodiversity Conservation. Report, DWLBC 2003/4.

Faneca Sànchez, M, Gunnink, JL, Van Baaren, ES, Oude Essink, GHP, Siemon, B, Auken, E, et al. (2012). Modelling climate change effects on a Dutch coastal groundwater system using airborne electromagnetic measurements. Hydrology and Earth System Sciences, 16, 4499–4516. https://doi.org/10.5194/hess-16-4499-2012

Fitzpatrick, A, Cahill, K, Munday, T and Berens, V, (2009), Informing the Hydrogeology of Coffin Bay, South Australia, through the Constrained Inversion of TEMPEST AEM Data, CSIRO: Water for a Healthy Country National Research Flagship CSIRO Report Number: P2009/300

Goebel, M, Knight, R, and M. Halkjær(2019) Mapping saltwater intrusion with an airborne electromagnetic method in the offshore coastal environment, Monterey Bay, California. J. Hydrol.: Regional Studies., 23 (2019), Article 100602.

Jørgensen, F, Scheer, W, Thomsen, S, Sonnenborg, TO, Hinsby, K, Wiederhold, H, et al. (2012). Transboundary geophysical mapping of geological elements and salinity distribution critical for the assessment of future sea water intrusion in response to sea level rise. Hydrology and Earth System Sciences, 16, 1845–1862. https://doi.org/10.5194/hess-16-1845-2012

Kirkegaard, C, Sonnenborg, T, Auken, E, and Jørgensen, F. (2011) Salinity distribution in heterogeneous coastal aquifers mapped by airborne electromagnetics, Vadose Zone J., 10, 125–135.

Lane, R, (2000) Conductive unit parameters: summarising complex conductivity distributions. 70th Meeting, SEG, Calgary, Expanded Abstracts, Volume 1, Section EM 4.2, p. 328-331.

Lane, R and Pracilio, G, (2000) Visualisation of Sub-Surface Conductivity Derived From Airborne EM. SAGEEP 2000 Conference Proceedings

Lane R, (2002) Ground and Airborne Electromagnetic methods. In Geophysical and Remote Sensing Methods for Regolith Exploration. (Ed É Papp) pp. 53-79. CRC LEME Open File Report 144. CRC LEME, Perth.

Lee, KT and Stenning, L. (2006) Coffin Bay, South Australia TEMPEST Geophysical Survey-Acquisition and Processing Report, Fugro Airborne Surveys, 30pp.

Maurya, P, Auken, E and Bording, T. (2024). A New Compact, Portable, and Fast Transient Electromagnetic System for Rapid Subsurface Imaging – sTEMprofiler. NSG 2024 30th European Meeting of Environmental and Engineering Geophysics, Sep 2024, Volume 2024, p.1 – 5; https://doi.org/10.3997/2214-4609.202420099

Pedersen JB, Schaars FW, Christiansen AV, Foged N, Schamper C, Rolf H, and Auken E. (2017) Mapping the fresh-saltwater interface in the coastal zone using high-resolution airborne electromagnetics. First Break. Aug 1;35(8).

Reid, J and Peters, G. (2015) Airborne electromagnetic survey for water supply planning - Cane River, Western Australia, ASEG Extended Abstracts, 2015:1, 1-4, https://doi.org/10.1071/ASEG2015ab165

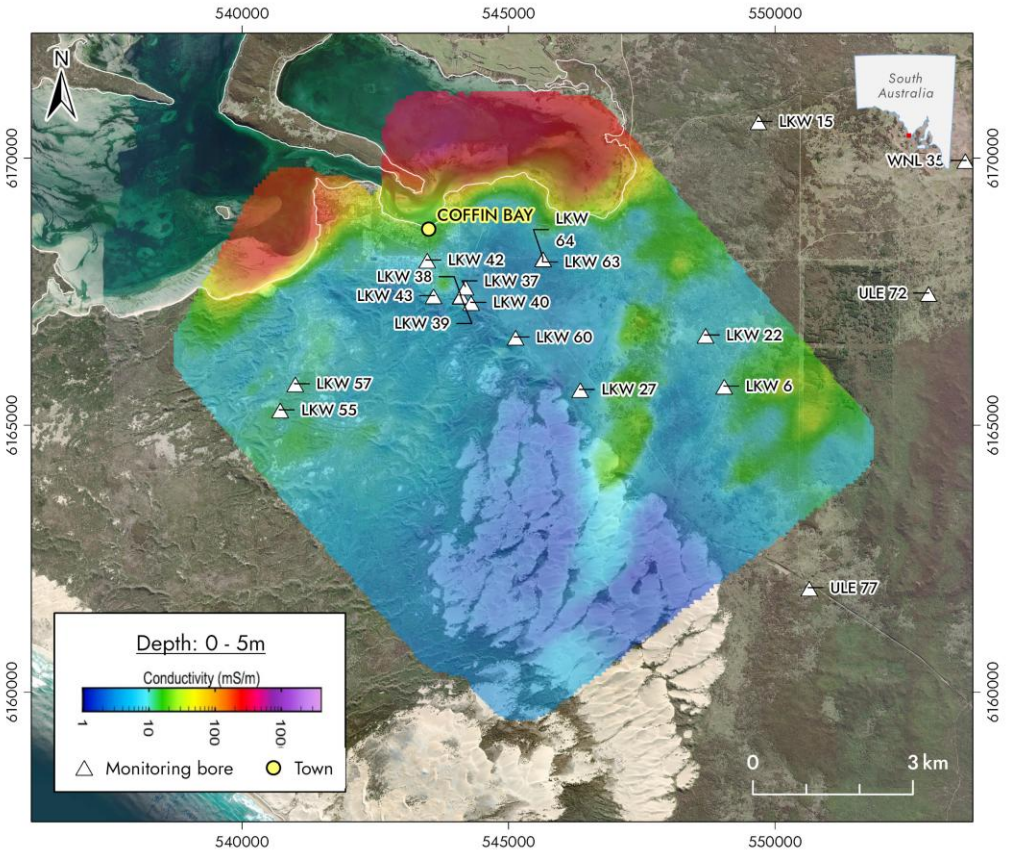
Somaratne, N, Zulfic, H, Swaffer, B and Ashman, G. (2009) Coffin Bay Groundwater Lens A-Resource Assessment. SA Water Technical Report; 63pp, DOI: 10.13140/RG.2.1.1334.3607.

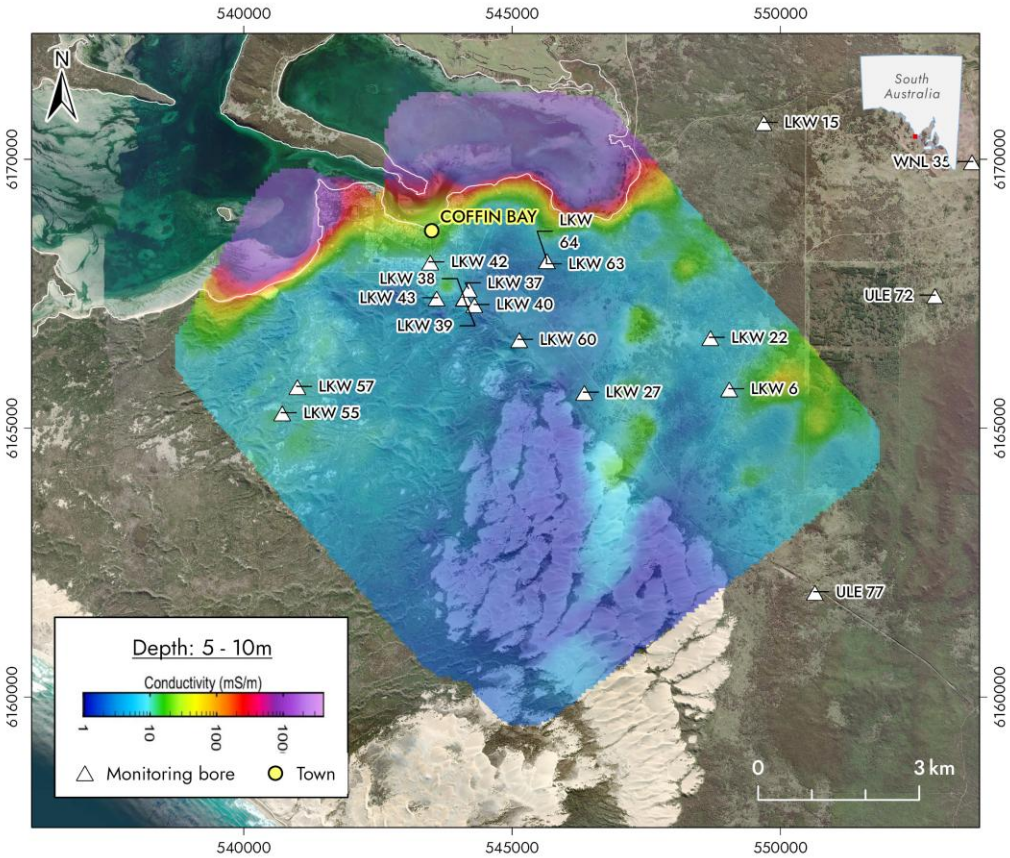
Teatini, P, Tosi, L, Viezzoli, A, Baradello, L, Zecchin, M and Silvestri, S. (2011). Understanding the hydrogeology of the Venice Lagoon subsurface with airborne electromagnetics, J. Hydrol., 411, 342–354.

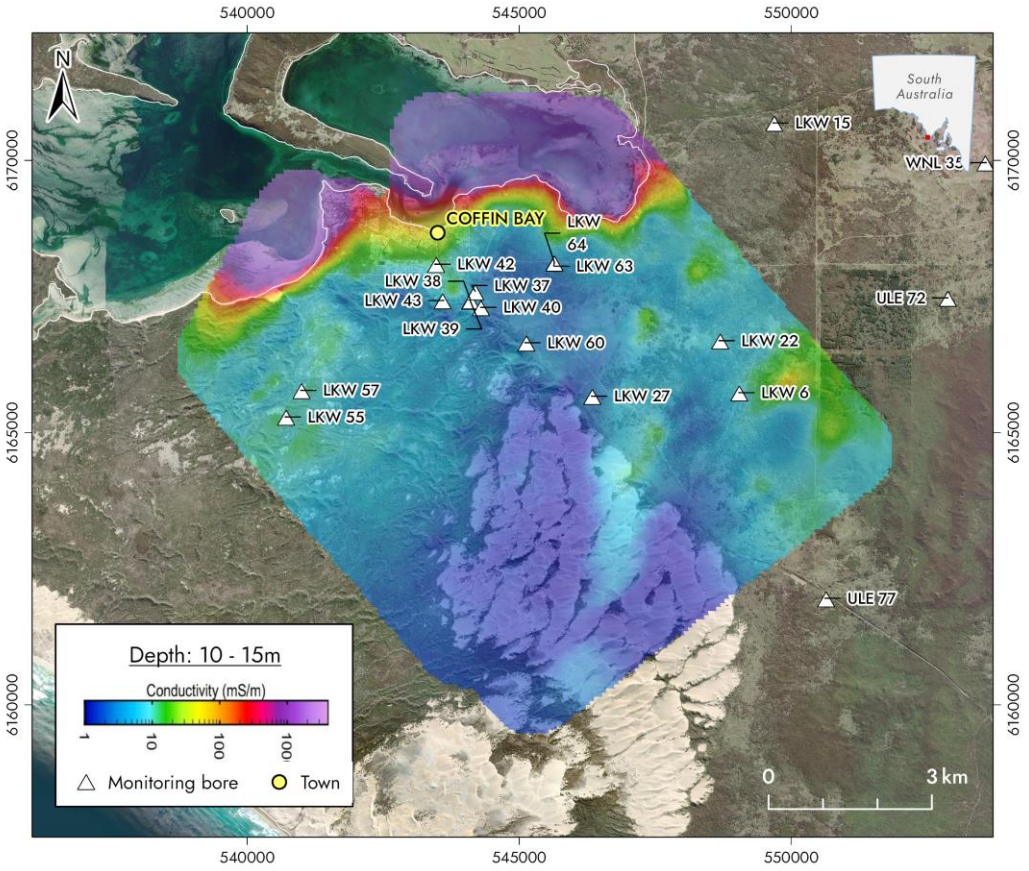
Ward, J.D., A.D. Werner and B. Howe (2009), Saltwater Intrusion in Southern Eyre Peninsula. Report developed through the Eyre Peninsula Groundwater, Allocation and Planning Project.62pp.

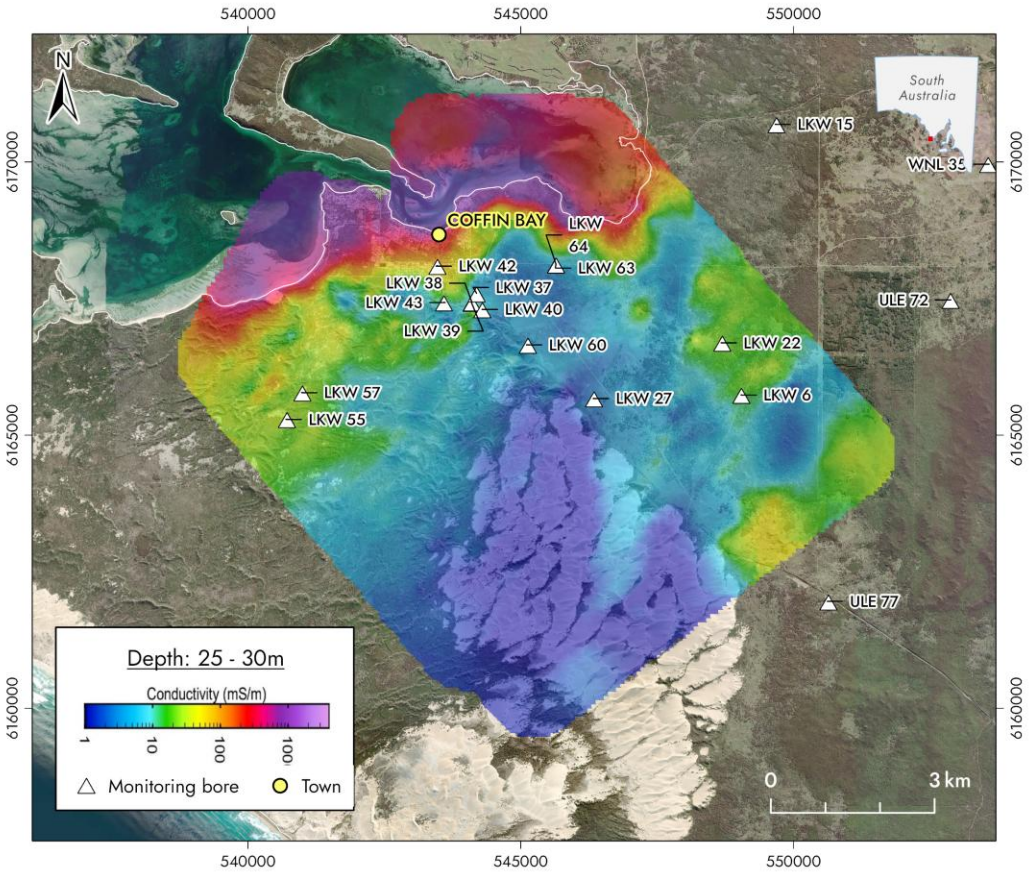
A.1 Appendices

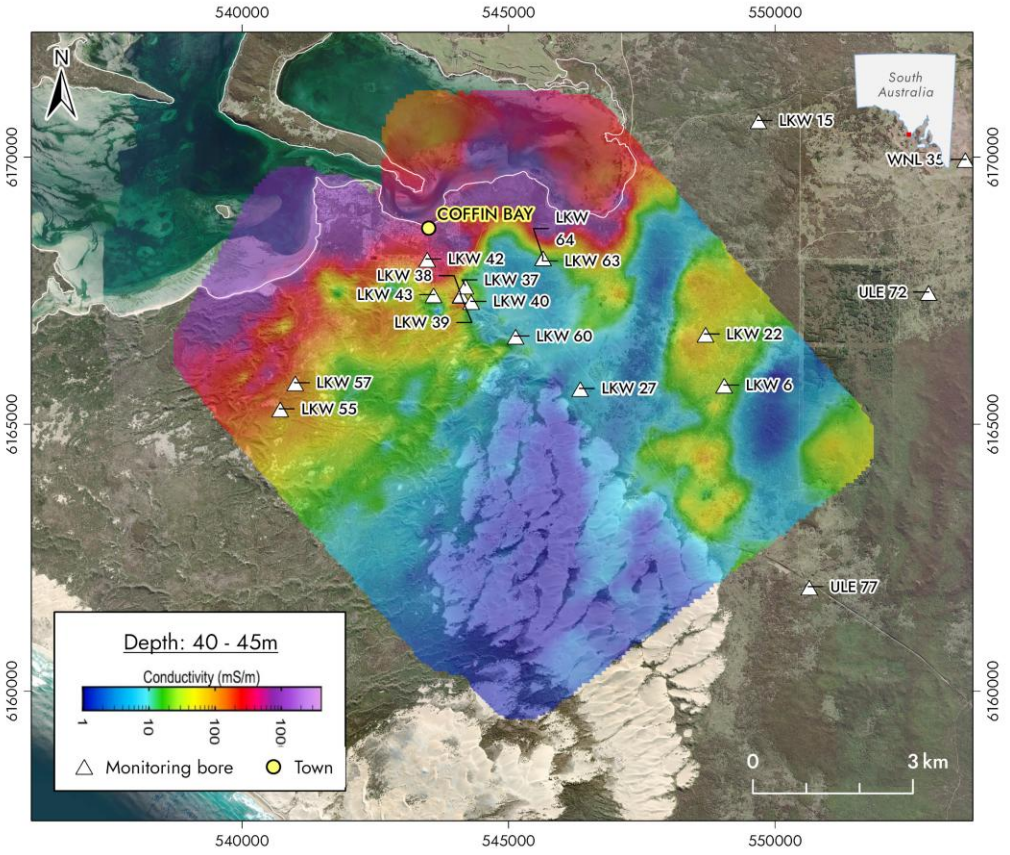
A.1.1 Representative Conductivity Depth (Below Ground Surface) Intervals

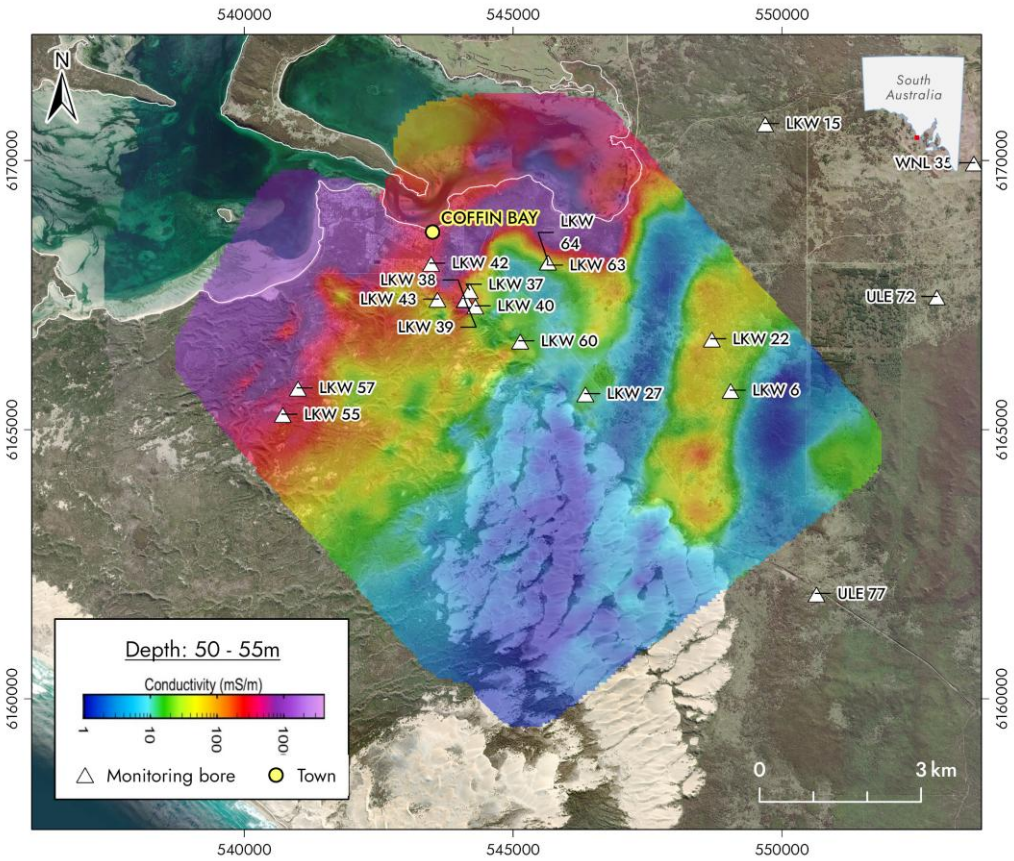


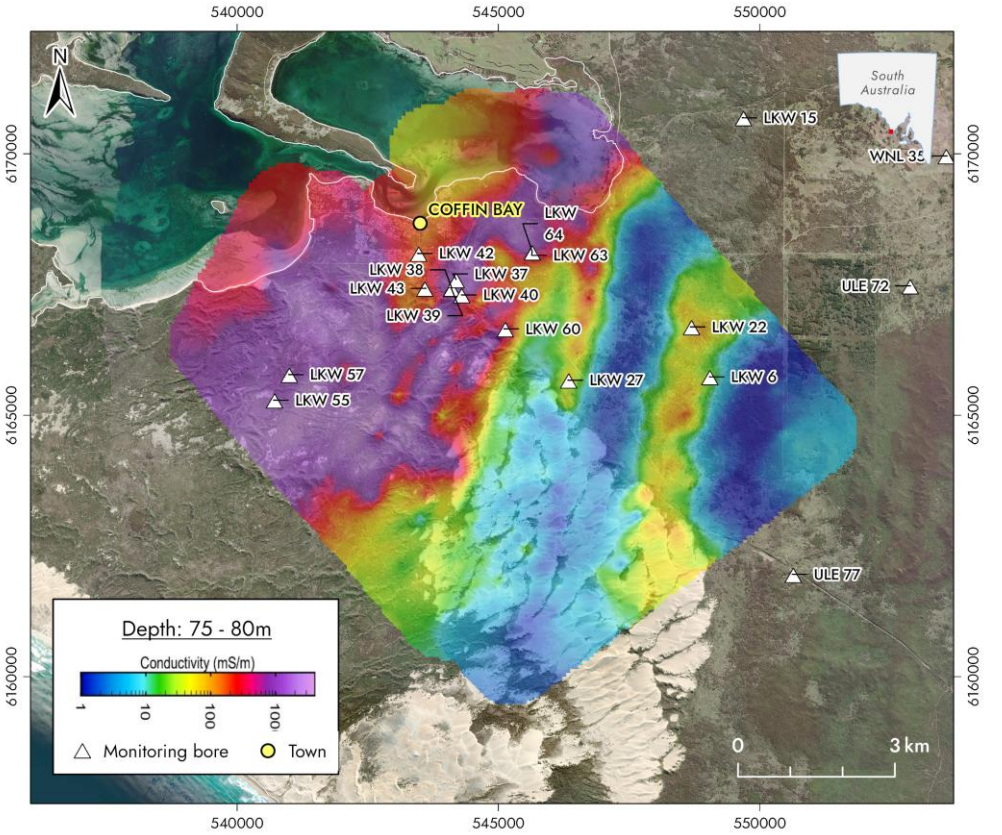


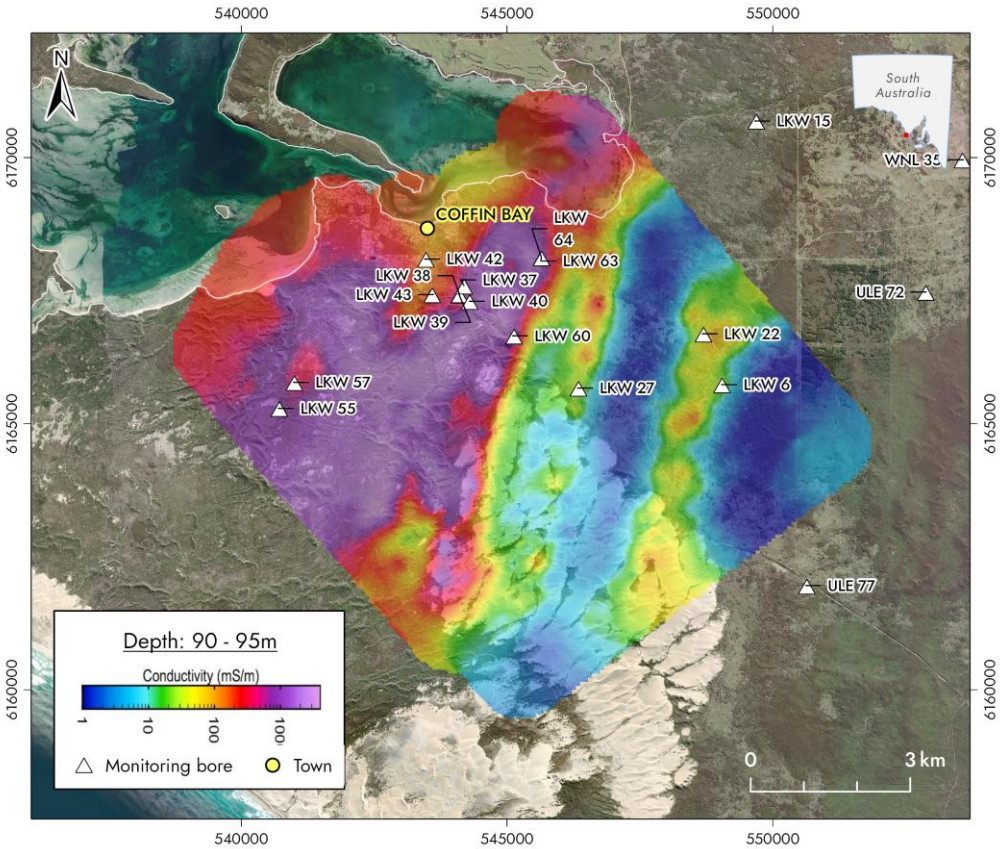

540000
545000
550000
6170000
6165000
6160000
N
South Australia
LKW 15
WNL 35
COFFIN BAY
LKW 64
LKW 42
LKW 63
LKW 38
LKW 37
LKW 43
LKW 40
LKW 39
ULE 72
LKW 60
LKW 22
LKW 57
LKW 27
LKW 6
LKW 55
ULE 77
Depth: 10 - 15m
Conductivity (mS/m)
1
10
100
100
Monitoring bore
Town
0
3 km


540000
545000
550000
6170000
6165000
6160000
N
South Australia
LKW 15
WNL 35
COFFIN BAY
LKW 64
LKW 42
LKW 63
LKW 38
LKW 37
LKW 43
LKW 40
LKW 39
ULE 72
LKW 60
LKW 22
LKW 57
LKW 27
LKW 6
LKW 55
ULE 77
Depth: 25 - 30m
Conductivity (mS/m)
1
10
100
100
Monitoring bore
Town
0
3 km


540000
545000
550000
6170000
6165000
6160000
N
South Australia
LKW 15
WNL 35
COFFIN BAY
LKW 64
LKW 42
LKW 63
LKW 38
LKW 37
LKW 43
LKW 40
LKW 39
LKW 60
LKW 22
ULE 72
LKW 57
LKW 55
LKW 27
LKW 6
ULE 77
Depth: 40 - 45m
Conductivity (mS/m)
1
10
100
100
Monitoring bore
Town
0
3 km


540000
545000
550000
6170000
6165000
6160000
N
South Australia
LKW 15
WNL 35
COFFIN BAY
LKW 64
LKW 42
LKW 63
LKW 38
LKW 37
LKW 43
LKW 40
LKW 39
LKW 60
LKW 22
ULE 72
LKW 57
LKW 55
LKW 27
LKW 6
ULE 77
Depth: 50 - 55m
Conductivity (mS/m)
1
10
100
100
Monitoring bore
Town
0
3 km

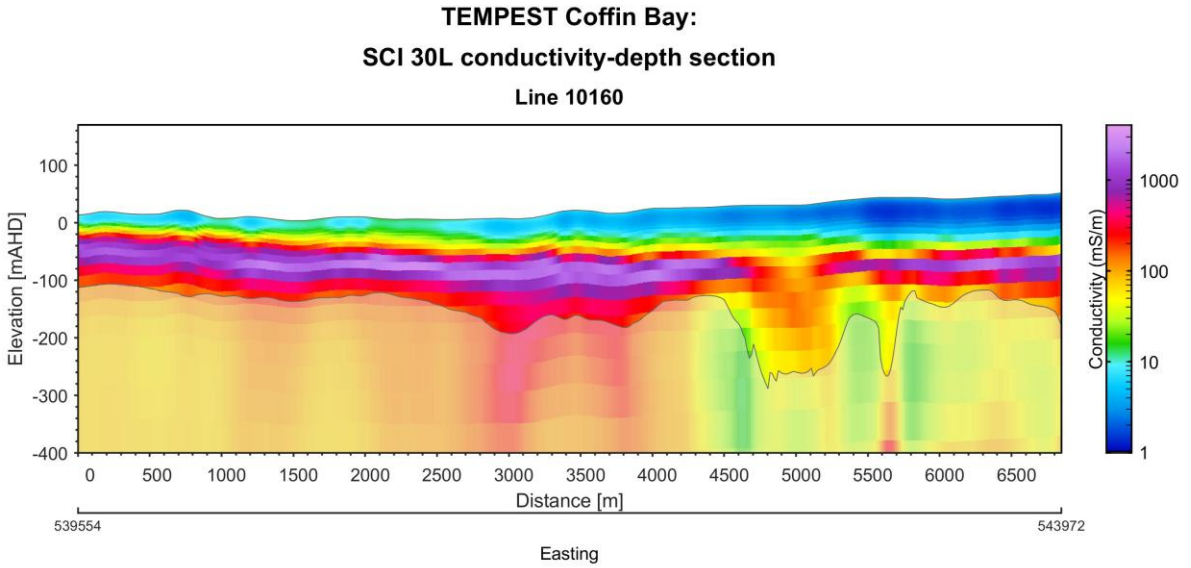

540000
545000
550000
6170000
6165000
6160000
N
South Australia
LKW 15
WNL 35
COFFIN BAY
LKW 64
LKW 42
LKW 63
LKW 38
LKW 37
LKW 43
LKW 40
LKW 39
ULE 72
LKW 60
LKW 22
LKW 57
LKW 55
LKW 27
LKW 6
ULE 77
Depth: 75 - 80m
Conductivity (mS/m)
1
10
100
100
Monitoring bore
Town
0
3 km

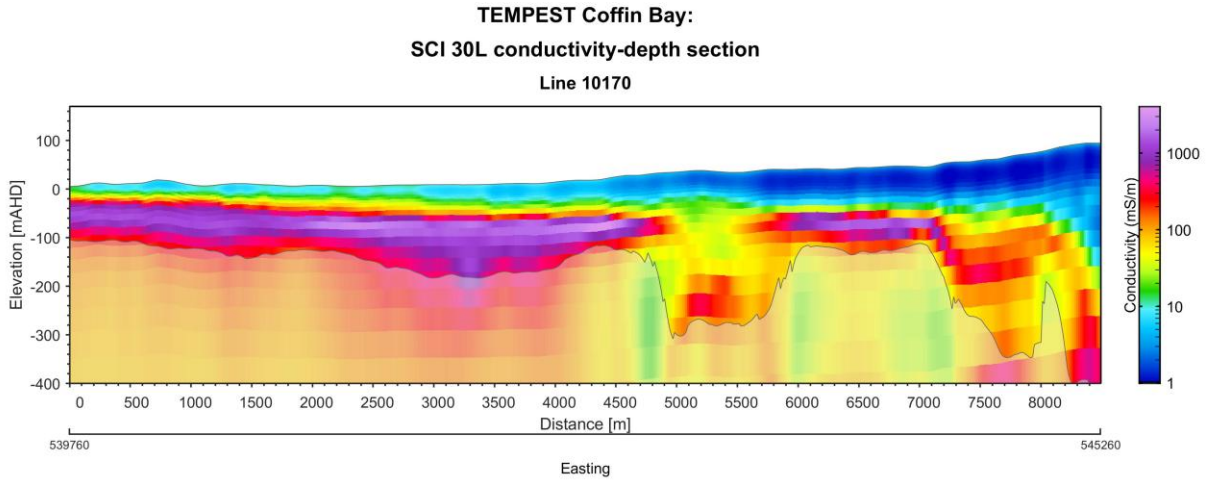

540000
545000
550000
6170000
6165000
6160000
N
South Australia
LKW 15
WNL 35
COFFIN BAY
LKW 64
LKW 42
LKW 63
LKW 38
LKW 37
LKW 43
LKW 40
LKW 39
ULE 72
LKW 60
LKW 22
LKW 57
LKW 55
LKW 27
LKW 6
ULE 77
Depth: 90 - 95m
Conductivity (mS/m)
1
10
100
100
Monitoring bore
Town
0
3 km

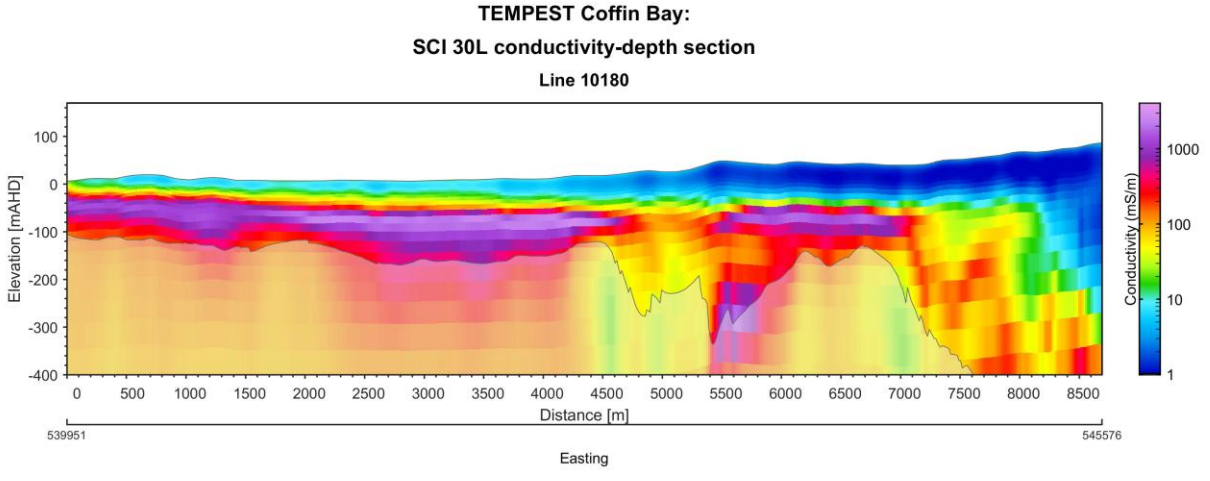
A.1.2 Conductivity Depth Sections

Sections presented are for each of the TEMPEST flight lines that have been inverted. The lines are shown in Figure 2-4.

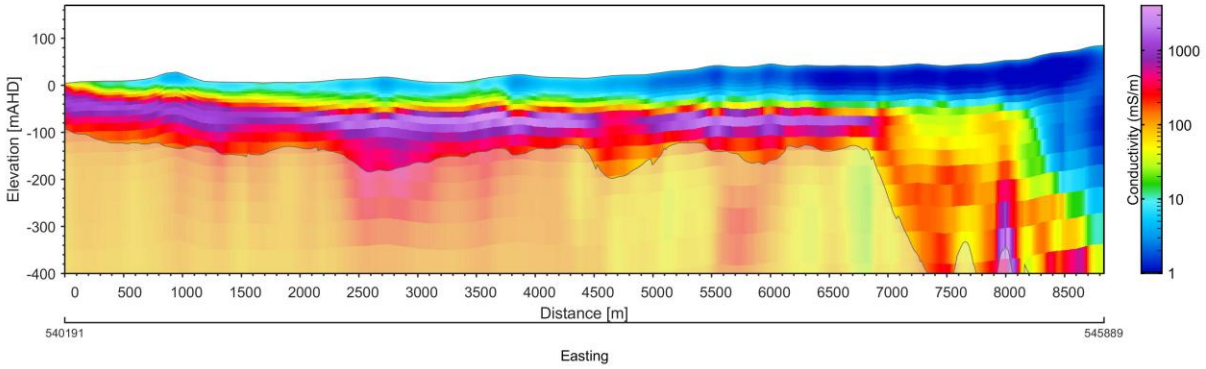
Smooth model (30 Layer) SCI inversion:



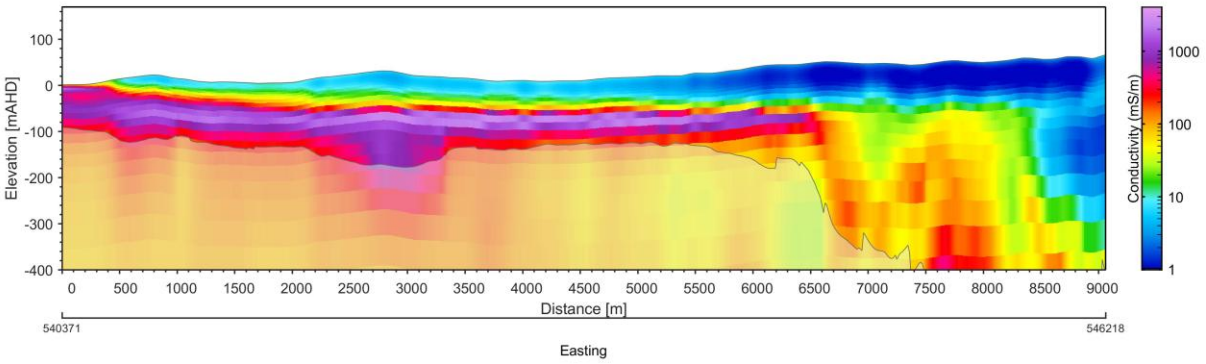




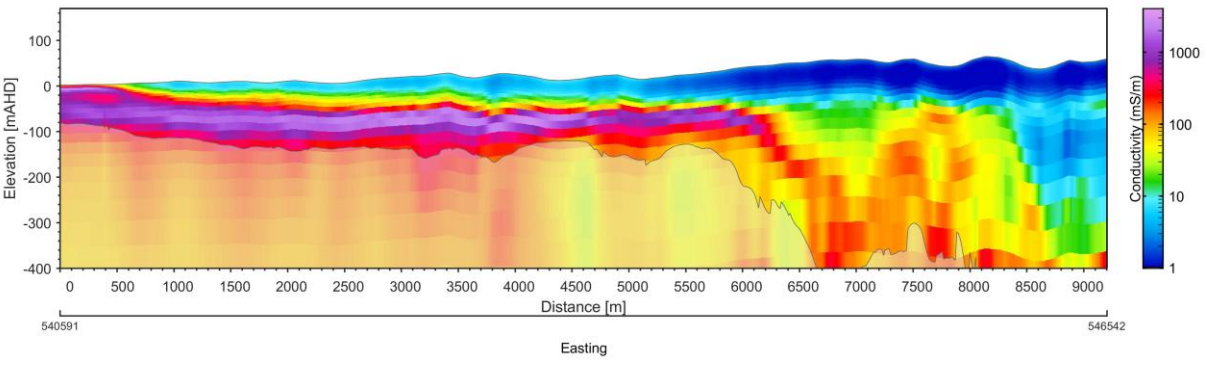
TEMPEST Coffin Bay:
SCI 30L conductivity-depth section
Line 10190



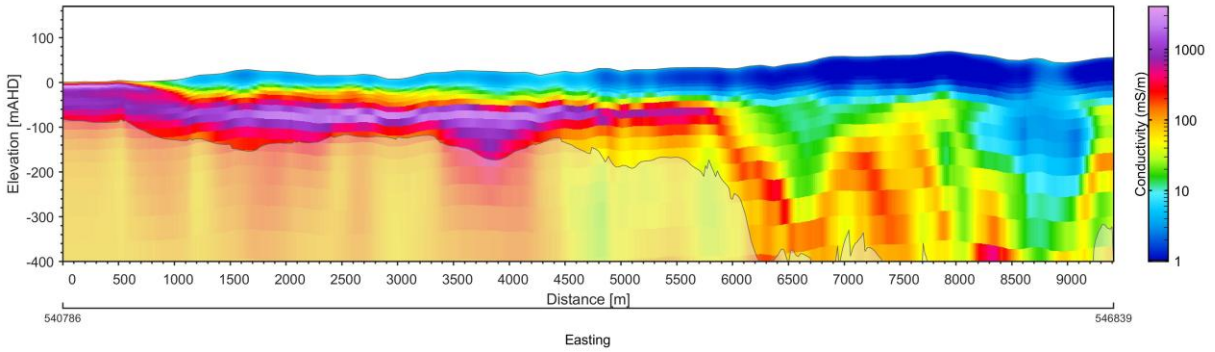
TEMPEST Coffin Bay:
SCI 30L conductivity-depth section
Line 10200



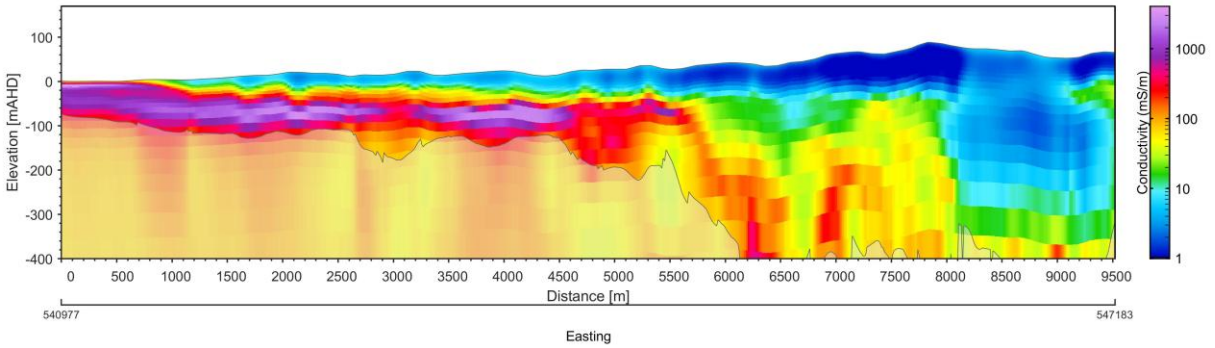
TEMPEST Coffin Bay:
SCI 30L conductivity-depth section
Line 10210



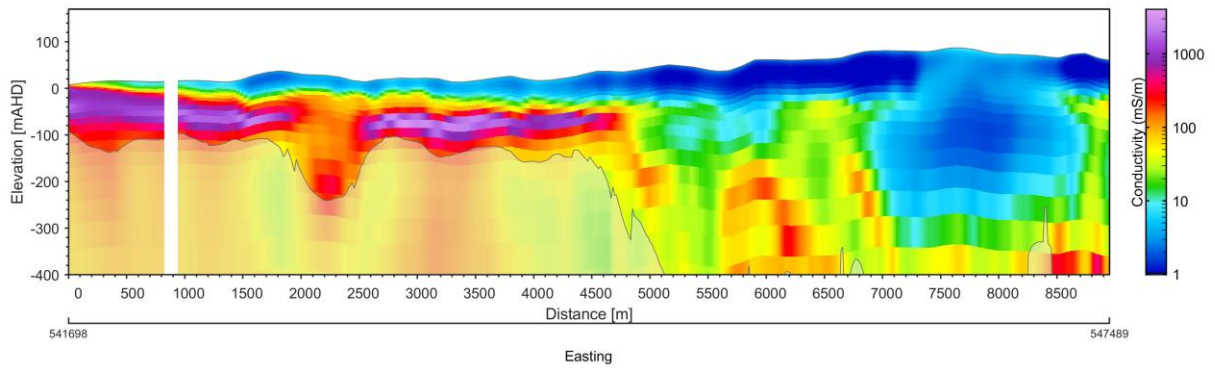
TEMPEST Coffin Bay:
SCI 30L conductivity-depth section
Line 10220



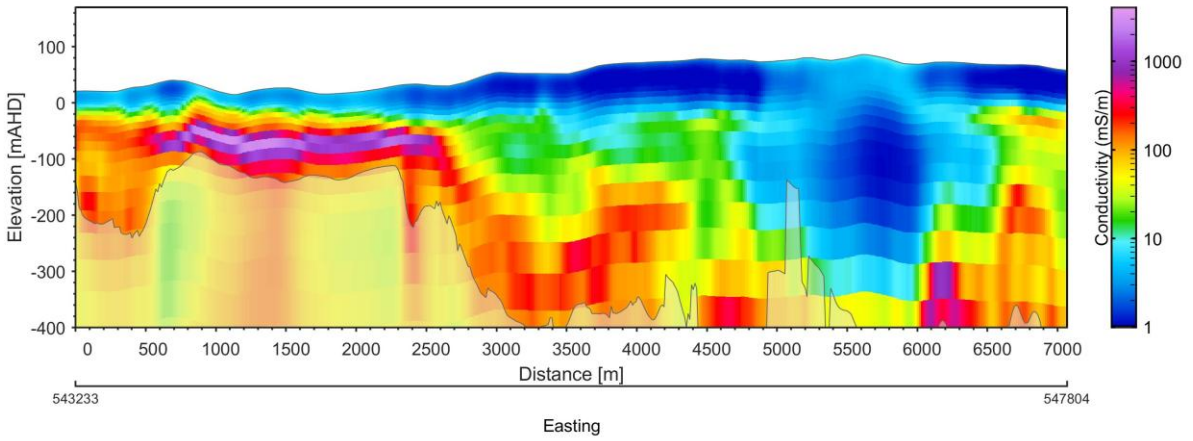
TEMPEST Coffin Bay:
SCI 30L conductivity-depth section
Line 10230



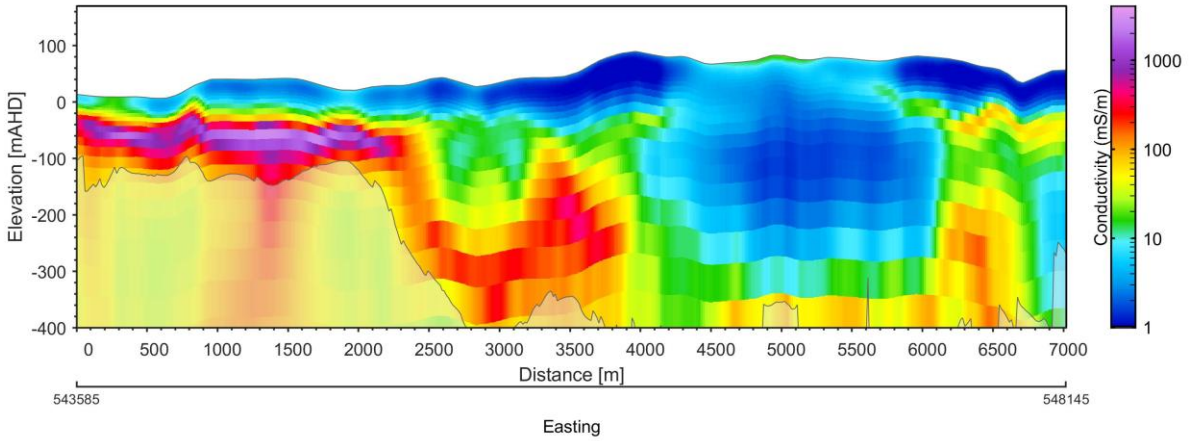
TEMPEST Coffin Bay:
SCI 30L conductivity-depth section
Line 10240



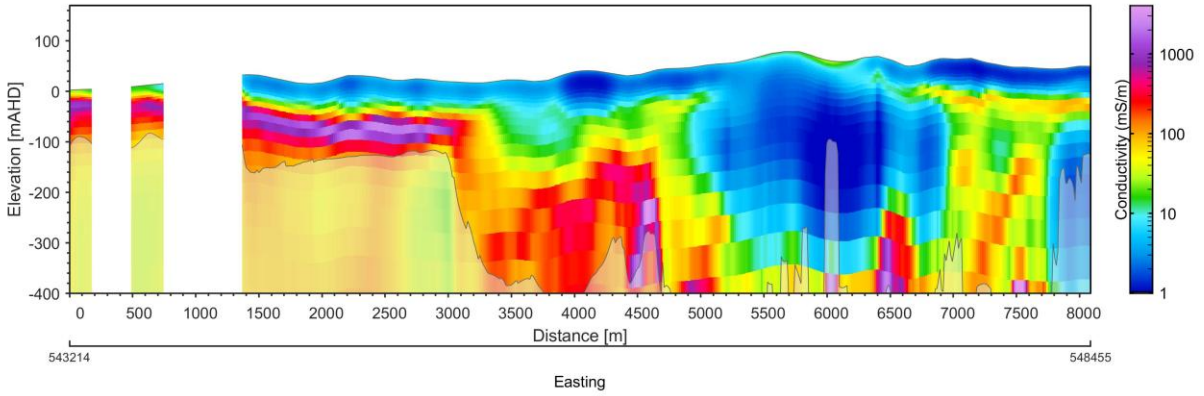
TEMPEST Coffin Bay:
SCI 30L conductivity-depth section
Line 10250



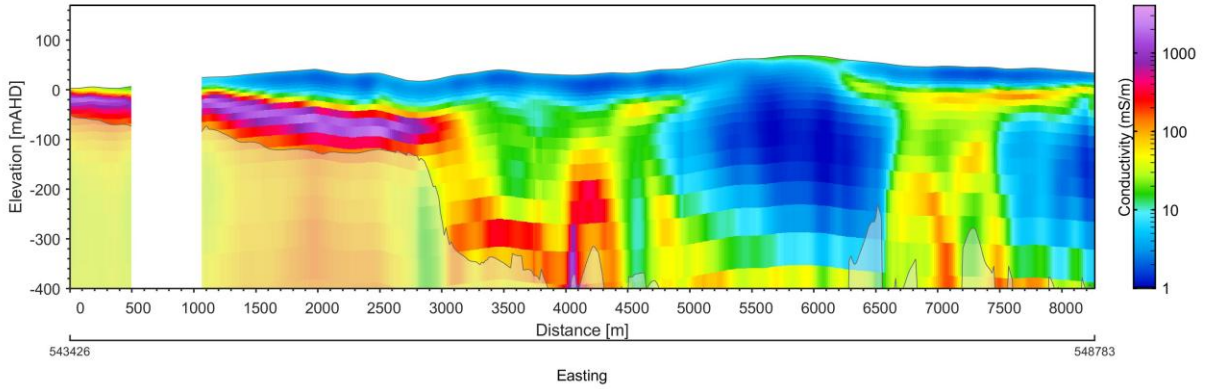
TEMPEST Coffin Bay:
SCI 30L conductivity-depth section
Line 10260



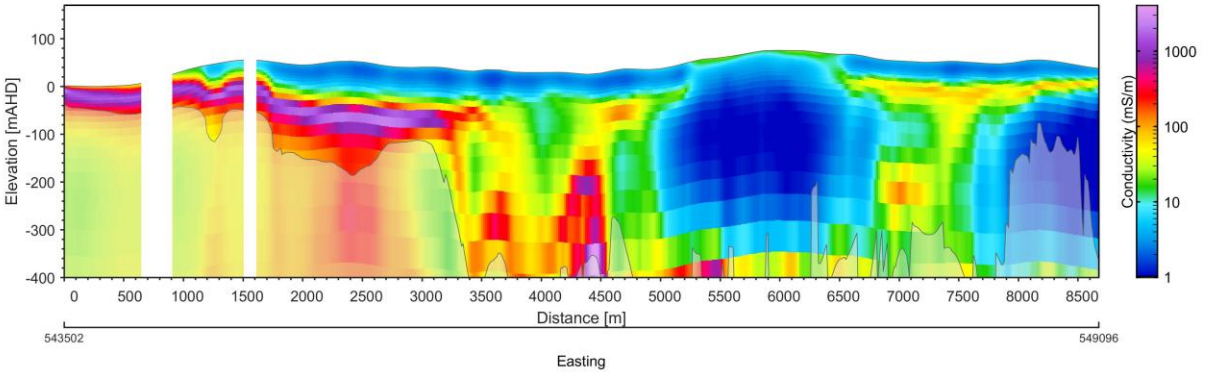
TEMPEST Coffin Bay:
SCI 30L conductivity-depth section
Line 10270



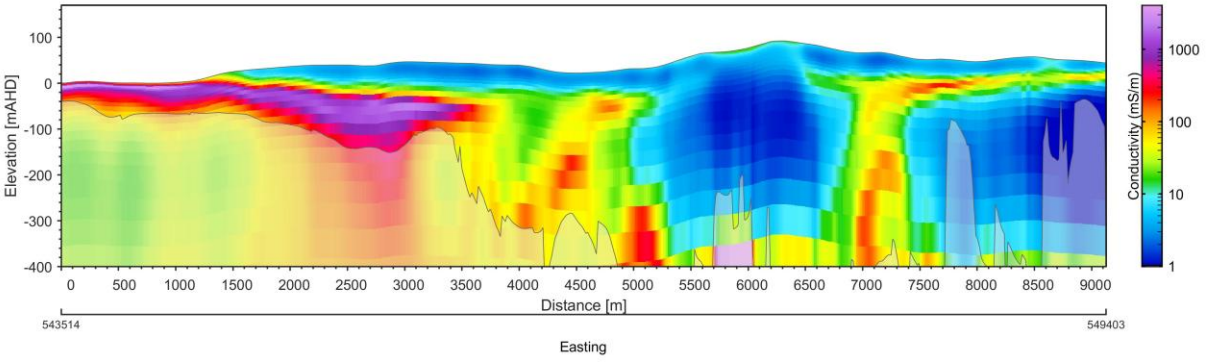
TEMPEST Coffin Bay:
SCI 30L conductivity-depth section
Line 10280



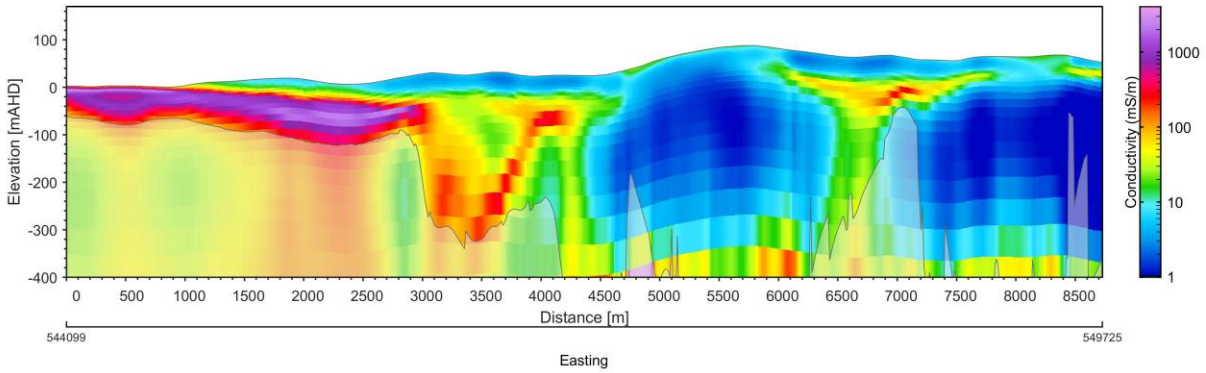
TEMPEST Coffin Bay:
SCI 30L conductivity-depth section
Line 10290



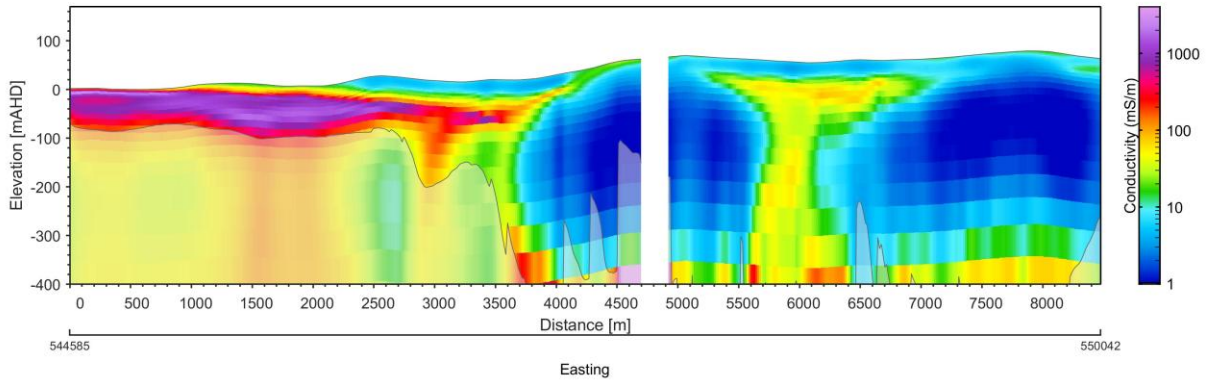
TEMPEST Coffin Bay:
SCI 30L conductivity-depth section
Line 10300



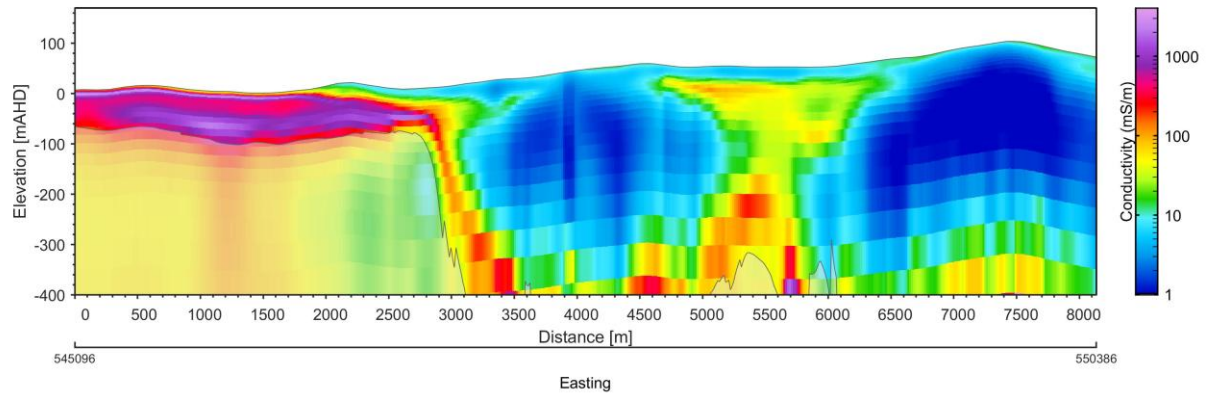
TEMPEST Coffin Bay:
SCI 30L conductivity-depth section
Line 10310



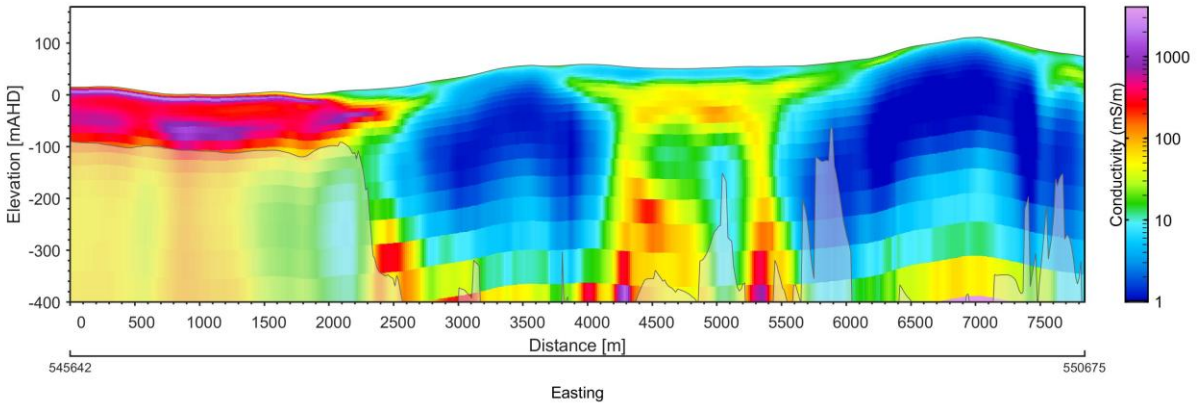
TEMPEST Coffin Bay:
SCI 30L conductivity-depth section
Line 10321



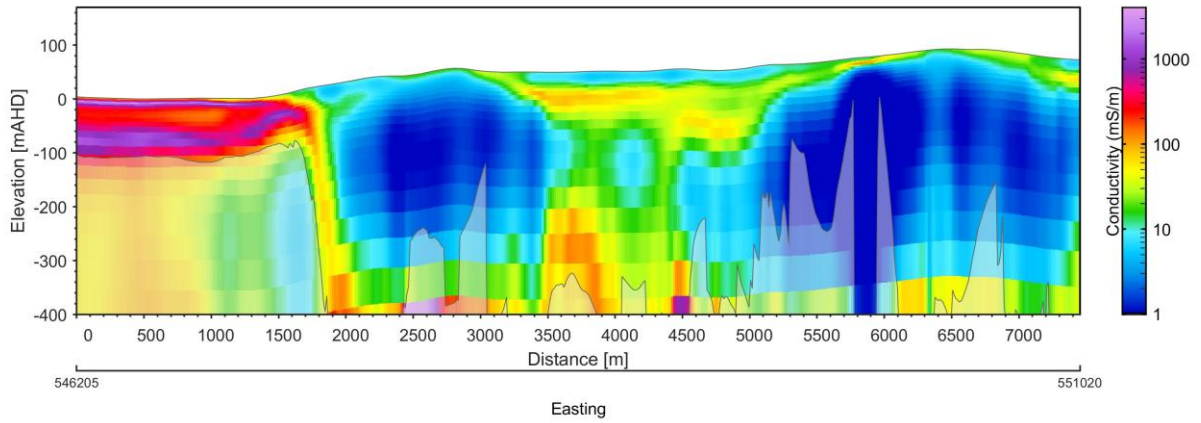
TEMPEST Coffin Bay:
SCI 30L conductivity-depth section
Line 10330



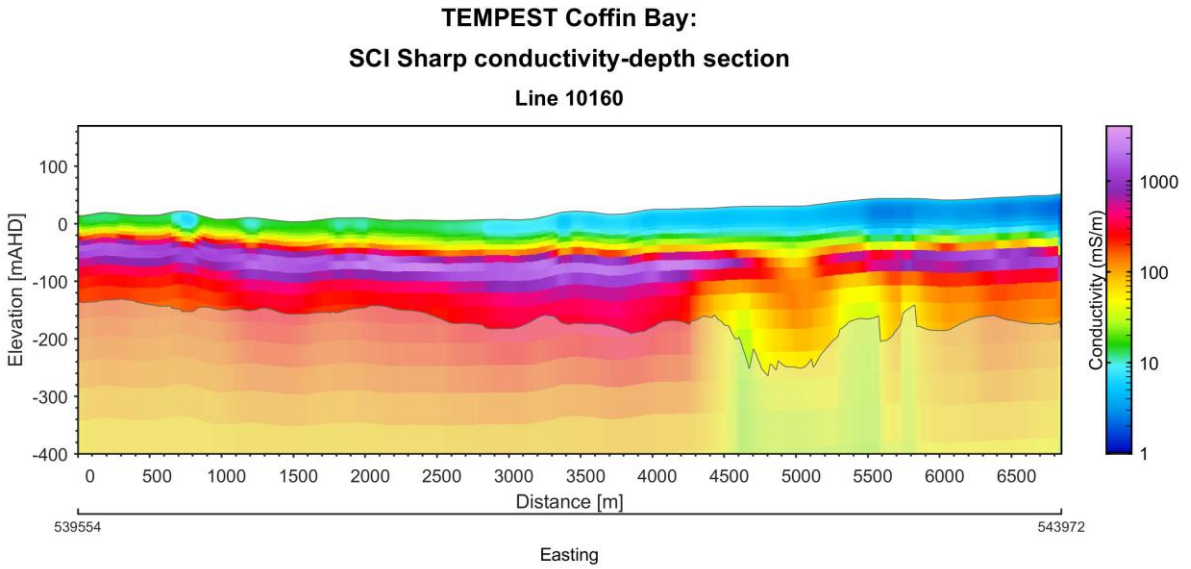
TEMPEST Coffin Bay:
SCI 30L conductivity-depth section
Line 10340

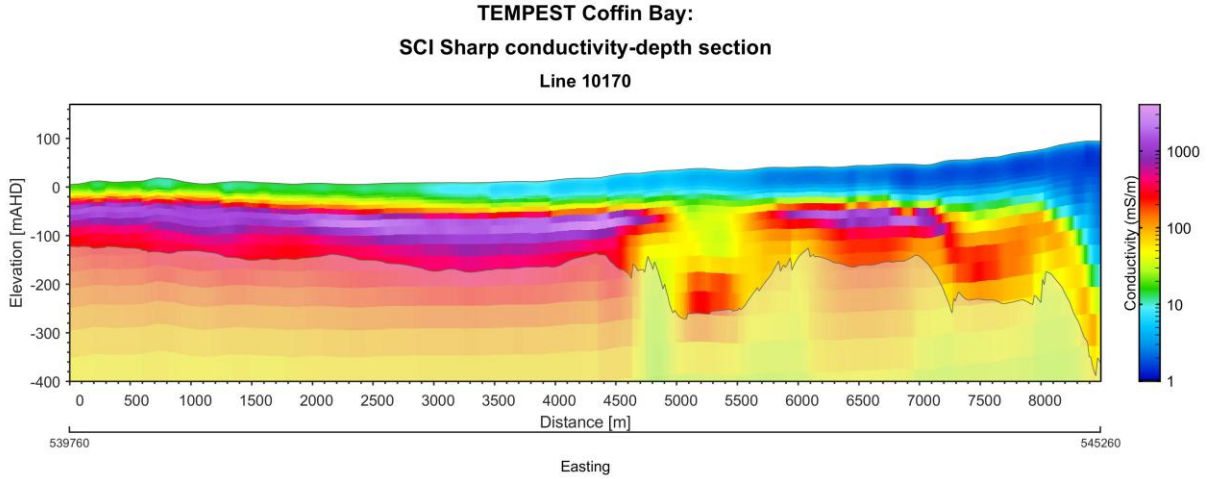


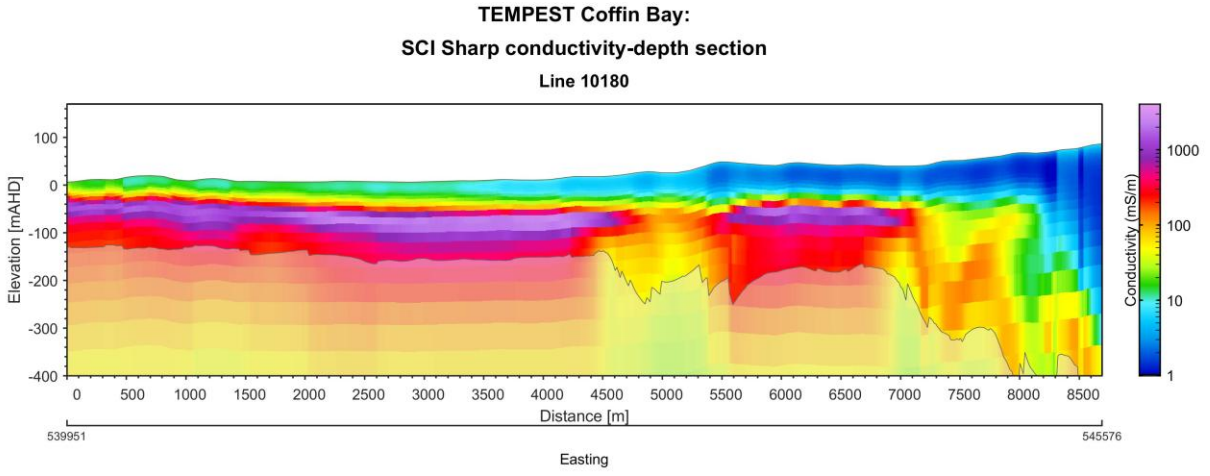
TEMPEST Coffin Bay:
SCI 30L conductivity-depth section
Line 10350



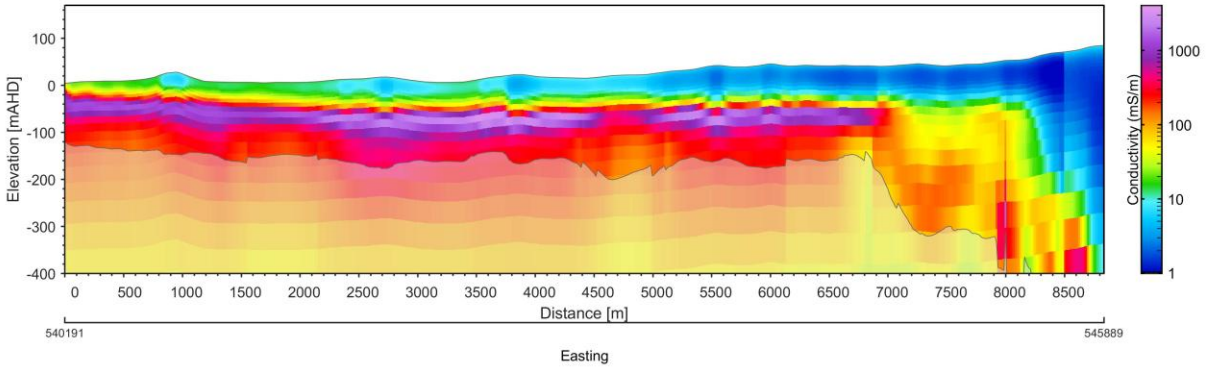
30 Layer sharp inversion SCI



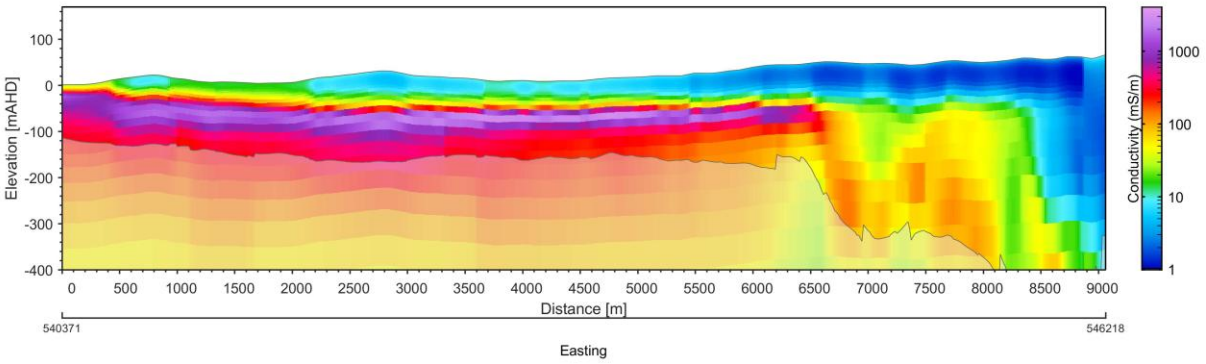




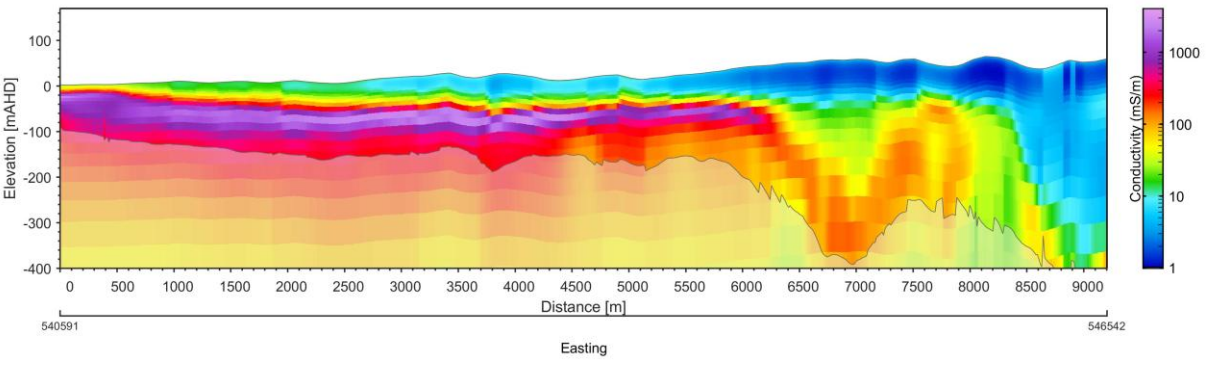
TEMPEST Coffin Bay:
SCI Sharp conductivity-depth section
Line 10190



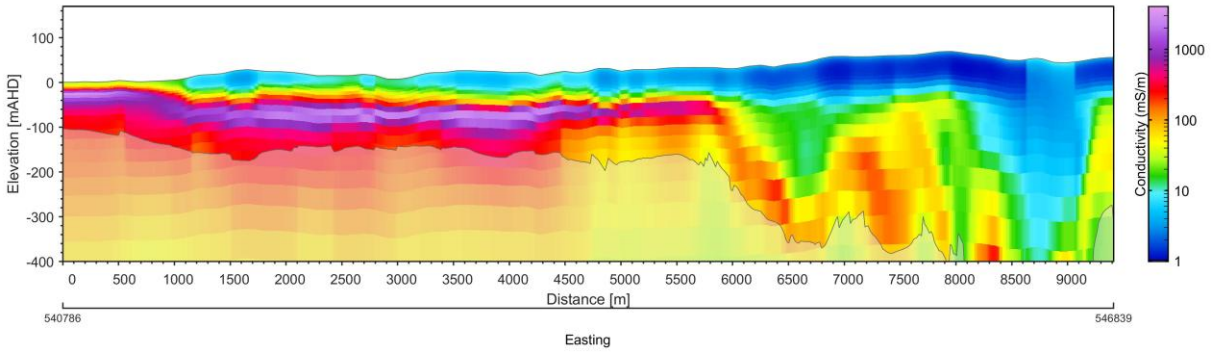
TEMPEST Coffin Bay:
SCI Sharp conductivity-depth section
Line 10200



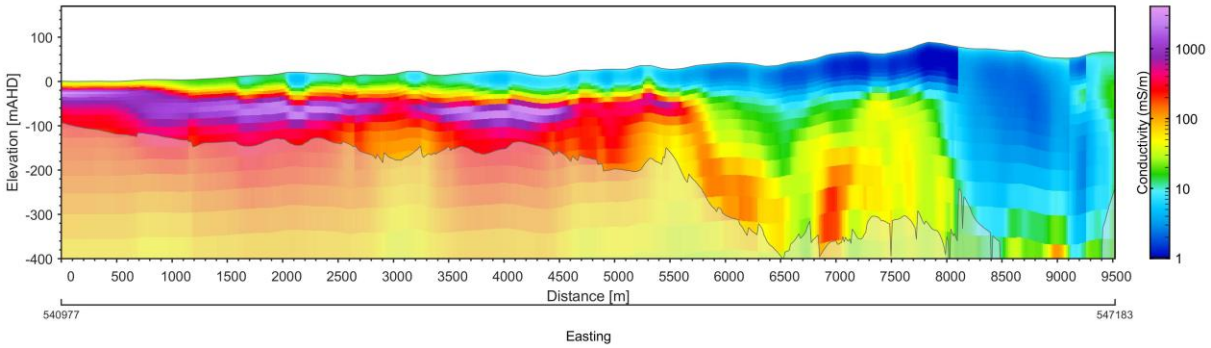
TEMPEST Coffin Bay:
SCI Sharp conductivity-depth section
Line 10210



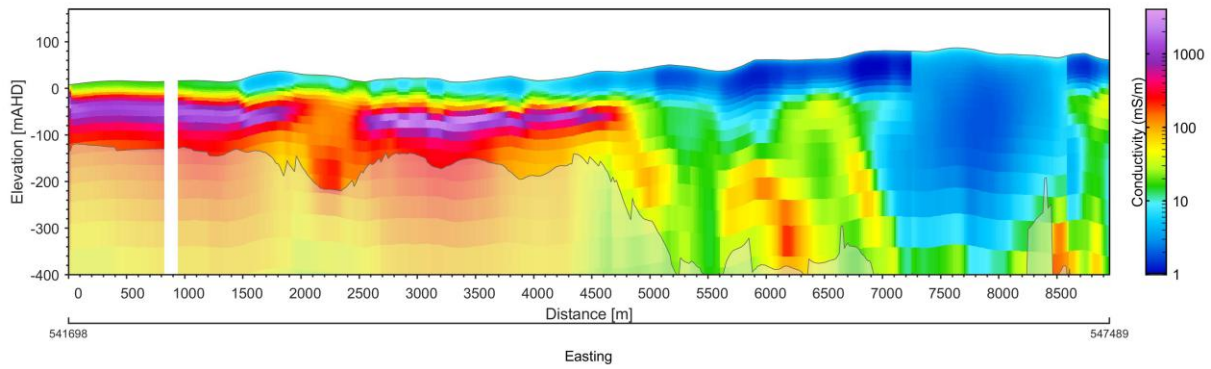
TEMPEST Coffin Bay:
SCI Sharp conductivity-depth section
Line 10220



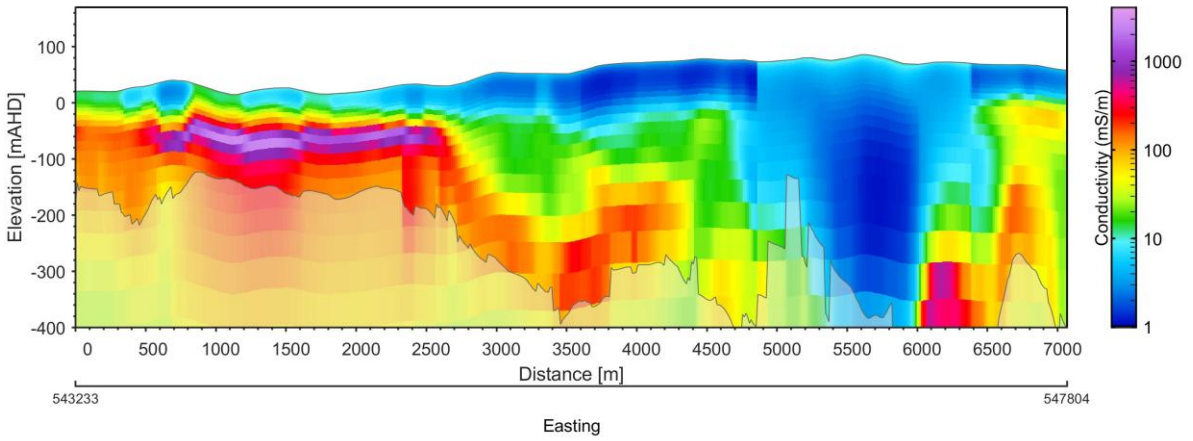
TEMPEST Coffin Bay:
SCI Sharp conductivity-depth section
Line 10230



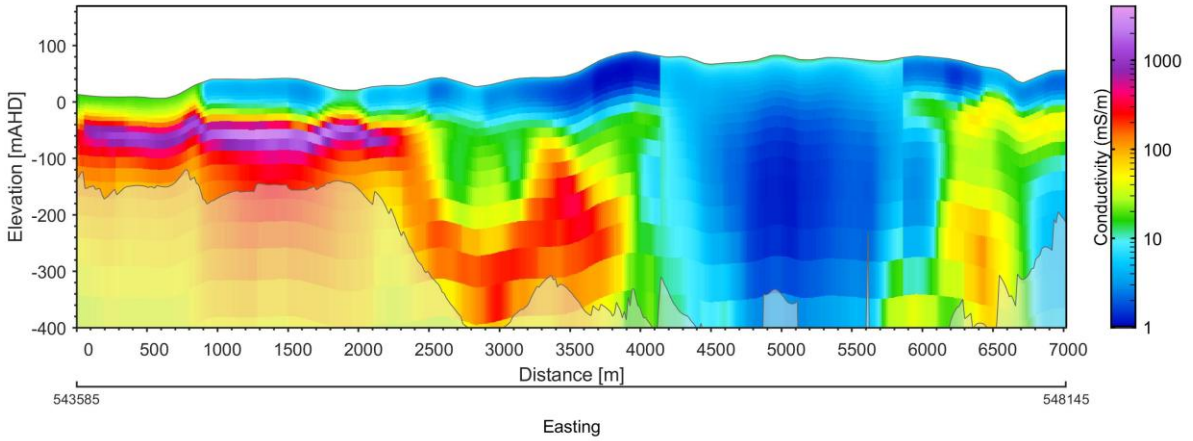
TEMPEST Coffin Bay:
SCI Sharp conductivity-depth section
Line 10240



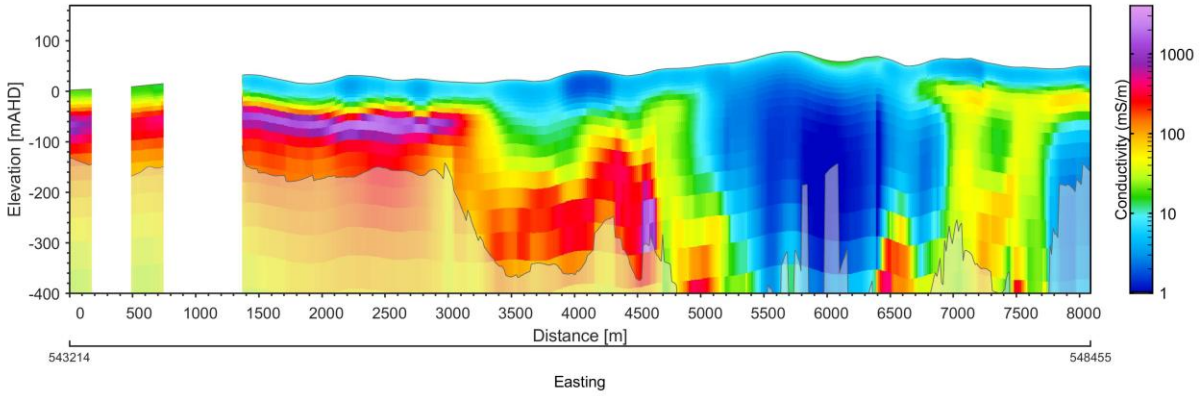
TEMPEST Coffin Bay:
SCI Sharp conductivity-depth section
Line 10250



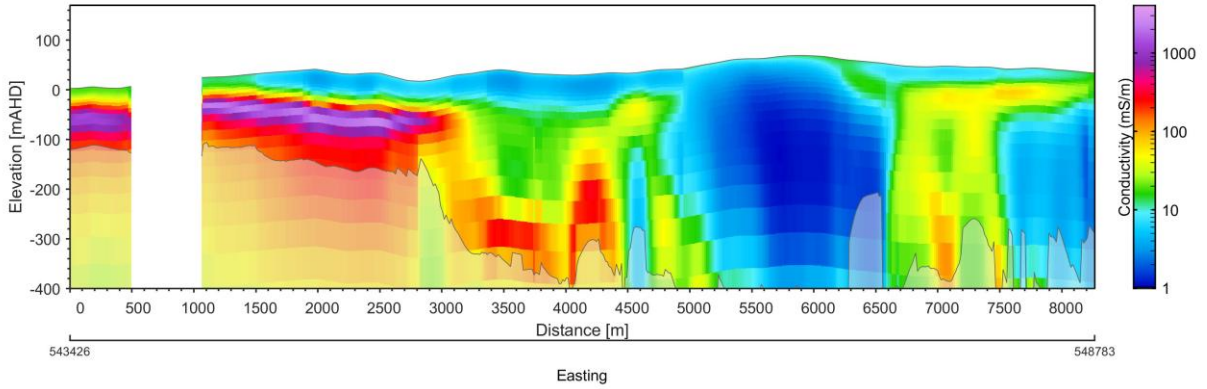
TEMPEST Coffin Bay:
SCI Sharp conductivity-depth section
Line 10260



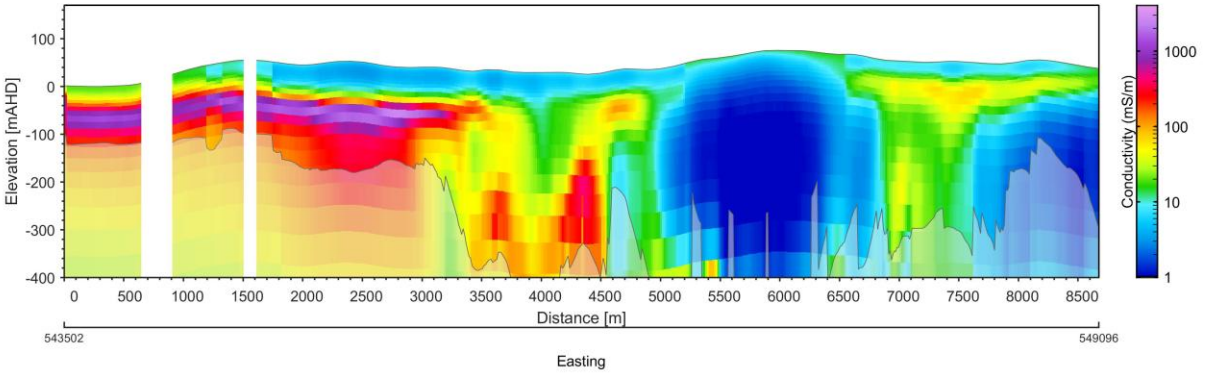
TEMPEST Coffin Bay:
SCI Sharp conductivity-depth section
Line 10270



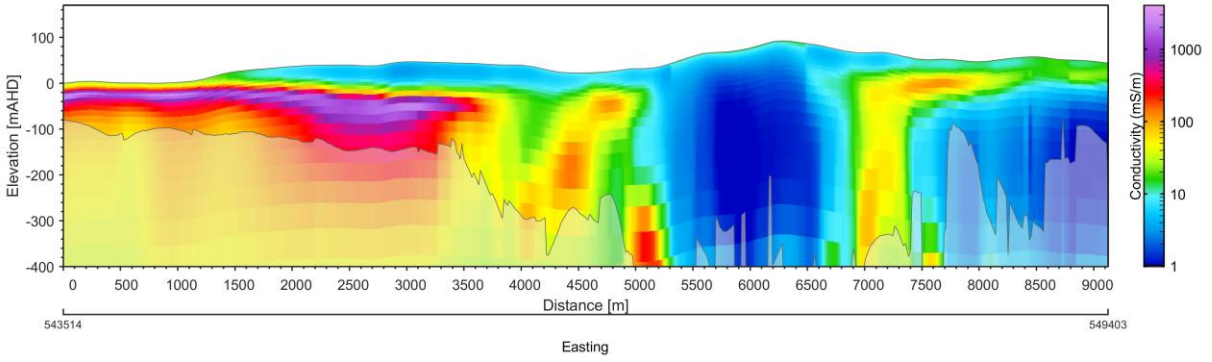
TEMPEST Coffin Bay:
SCI Sharp conductivity-depth section
Line 10280



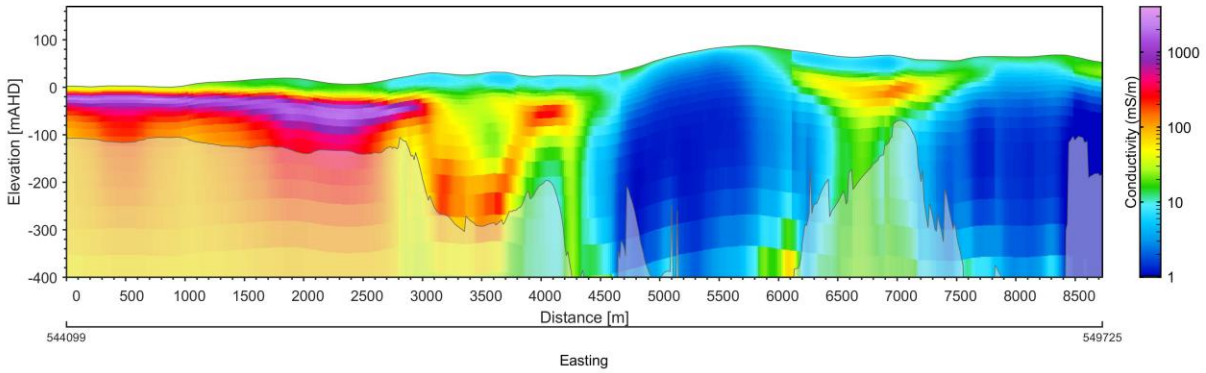
TEMPEST Coffin Bay:
SCI Sharp conductivity-depth section
Line 10290



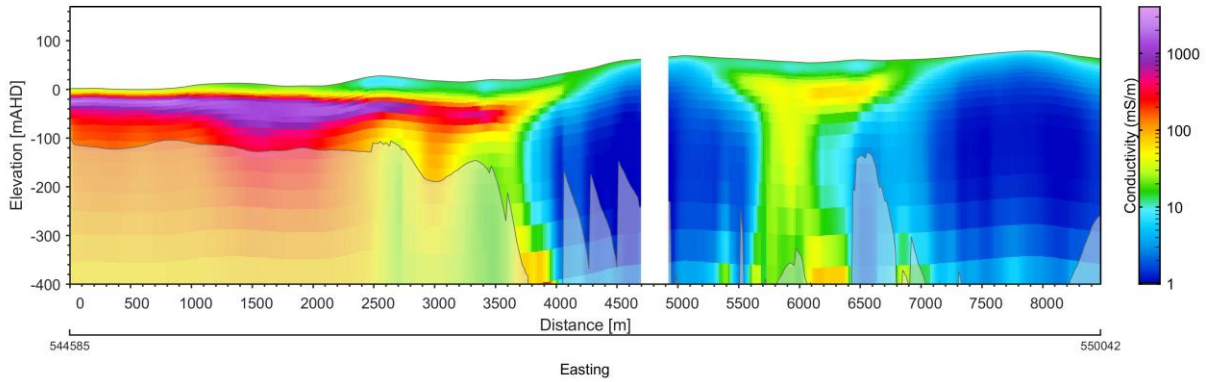
TEMPEST Coffin Bay:
SCI Sharp conductivity-depth section
Line 10300



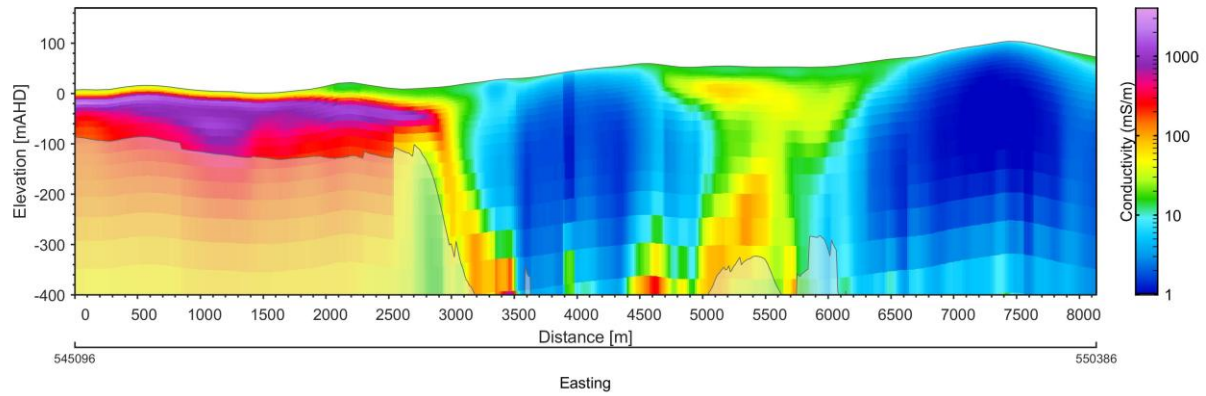
TEMPEST Coffin Bay:
SCI Sharp conductivity-depth section
Line 10310



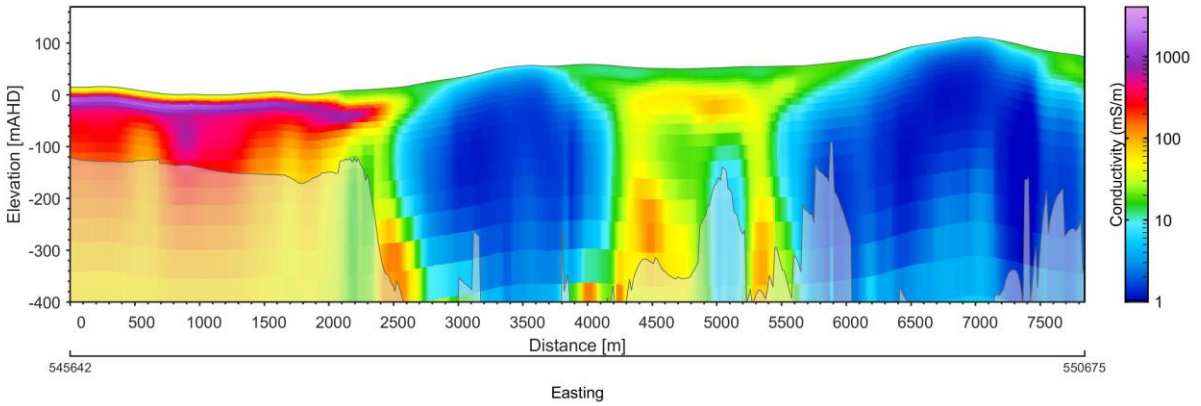
TEMPEST Coffin Bay:
SCI Sharp conductivity-depth section
Line 10321



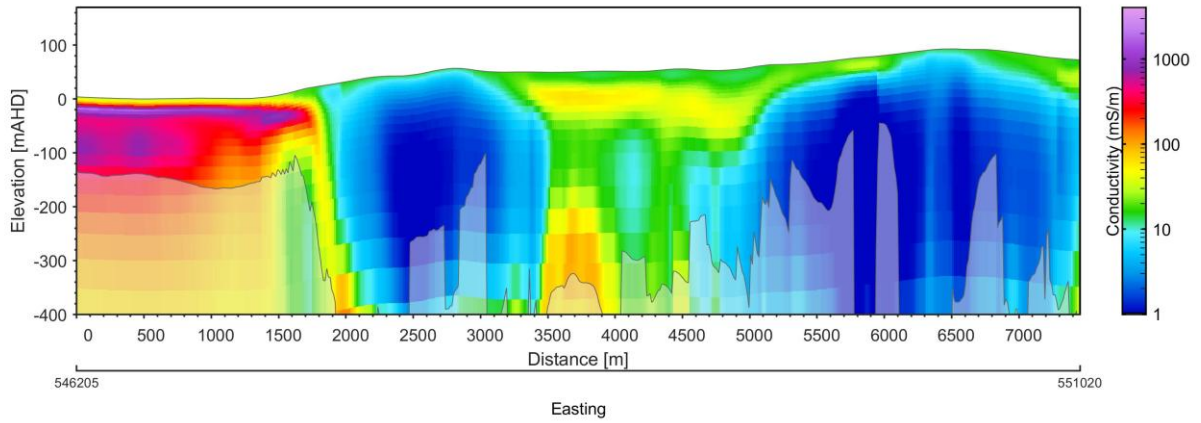
TEMPEST Coffin Bay:
SCI Sharp conductivity-depth section
Line 10330



TEMPEST Coffin Bay:
SCI Sharp conductivity-depth section
Line 10340



TEMPEST Coffin Bay:
SCI Sharp conductivity-depth section
Line 10350



As Australia's national science agency and innovation catalyst, CSIRO is solving the greatest challenges through innovative science and technology.

CSIRO. Unlocking a better future for everyone.

Contact us

1300 363 400
+61 3 9545 2176
csiro.au/contact
csiro.au

For further information:

CSIRO Mineral Resources
Tim Munday
+61 418221311
tim.munday@csiro.au